Ph.D. Dissertation

EFFECTS OF USER BODY SHADOWING IN INDOOR WIRELESS CHANNEL BASED ON RAY TRACING

광선 추적 기법에 기반한 실내 무선 채널에서의 사용자 쉐도잉 영향

AUGUST 2015

Department of Electrical Engineering and
Computer Science
College of Engineering
Seoul National University

Jae-Hoon Jung

EFFECTS OF USER BODY SHADOWING IN INDOOR WIRELESS CHANNEL BASED ON RAY TRACING

지도교수 김 성 철

이 논문을 공학박사 학위논문으로 제출함
2015년 8월

서울대학교 대학원
전기 · 컴퓨터공학부
정 재 훈

정재훈의 박사 학위논문을 인준함
2015년 7월

위 원 장 _____ 김 남 수 (인)

부위원장 _____ 김 성 철 (인)

위 원 _____ 심 병 효 (인)

위 원 _____ 김 영 록 (인)

위 원 _____ 김 용 화 (인)

Abstract

EFFECTS OF USER BODY SHADOWING IN INDOOR WIRELESS CHANNEL BASED ON RAY TRACING

Jae-Hoon Jung
Department of Electrical Engineering and Computer Science
The Graduate School
Seoul National University

In this dissertation, the effects of user body on radio wave propagation in indoor wireless channels are analyzed. The user who is nearly always being close to mobile device influences very strongly and consistently on propagation channel. Therefore, exclusively focusing on the user body separately from other bodies, the shadowing effects caused by the user are investigated at 2.4 GHz by using the uniform theory of diffraction (UTD) and the ray-tracing technique.

First of all, the user body shadowing (UBS) effects on a single ray path are investigated deterministically by using the UTD. The UTD scattering

solutions for diffraction at a smooth convex surface are adopted to analyze the effects of user body modeled as a circular cylinder. The UTD-based model for a single ray path is defined as the relative received signal power according to the relative position of user, which is validated by measurements in an anechoic chamber.

The validated UTD-based model is combined with the indoor ray-tracing technique in order to examine the UBS effects on multipath channels. Since the ray-tracing provides not only the powers of multipaths but also their angular profiles, it is possible to apply the UTD single path model according to the relationship between the user's position and the direction of rays. This combination method is also verified by in-building measurements.

In realistic communications, however, the user's position can be neither fixed at any one value and nor can its exact value be provided to systems in real time. Thus, a statistical analysis for the UBS is conducted taking into consideration the randomness of user's position. First, the K-factor, defined as the ratio of the power in the dominant path and the sum of the powers in the other paths, is proposed as the most significant factor to determine the UBS effects. Because the UBS effects considerably depend on the extent of the dominant path and whether the dominant path is blocked. As a result, the distributions of total power losses caused by the UBS are link-by-link modeled by Nakagami-*m* distributions. Additionally, the estimated parameter *m* is proposed as a function of K-factor.

Finally, the enhanced UBS stochastic model is proposed based on the

bimodal characteristics of UBS. The UBS model based on Nakagami-*m* distribution has a drawback of inaccuracies for the links with high K-factor because the distribution of total UBS losses for links with high K-factors has a bimodal shape that has two peaks in its histogram. Therefore, the distributions of total UBS losses were classified into unimodal and bimodal groups with the quantitative decision criterion of K-factor. For the unimodal model, Rician distribution is used to achieve the best accuracy, whereas Gaussian mixture model is exploited for the bimodal UBS model. The validity of these proposed models is verified using the ray-tracing simulation in various indoor environments.

Keywords: Ray-tracing, Uniform theory of diffraction, User body shadowing, Indoor wireless channel, Bimodal distribution

Student Number: 2008-20973

Contents

List of Tables

List of Figures

Chapter 1. Introduction

1.1 Indoor Wireless Propagation Channel

In wireless communication systems, it is very important to model the underlying propagation channel correctly because radio propagation properties significantly affect the system performance. The received signal power especially needs to be predicted accurately for the determination of many system specifications such as service coverage and transmission power [1]. In particular, indoor wireless communication systems request the accurate prediction of the received signal strength because they have the lower transmission power and the smaller coverage than outdoor systems. However, it is considerably complex to predict indoor wireless channels, so-called 'site-specific channels', due to high dependency on local environments such as building structures, wall materials, and furniture [2]. Relating to the indoor propagation channel, many studies based on experimental [2-7] and theoretical [8-10] approaches have been reported for decades.

Ray-tracing technique is one of the popular theoretical methods to deterministically analyze propagation channels [10-12]. The ray-tracing technique assumes that radio waves can be modeled as a large number of rays. The propagation of a ray is predicted based on geometrical optics (GO). In GO, a ray propagates straight in free space and its direction changes by specular reflection, diffraction, and refraction phenomena which severely

depend on surrounding objects. The radio wave characteristics of traced rays are calculated by electromagnetic theory. Thus, the ray-tracing is implemented as a computer simulation with the input of actual geometrical data. Consequently, the ray-tracing technique is more efficient than the physical measurements to characterize the site-specific channels. Two most popular ray-tracing techniques are the image-based method and the shoot-and-bounce ray (SBR) method [1]. Many researches on the ray-tracing algorithms and the corresponding performance measures have been published [13-17].

1.2 User Body Effects on Wireless Propagation Channel

The ray-tracing technique can provide the reliable prediction for a stationary channel in which both the transmitter and receiver are fixed and the surrounding environments are also unchanged. However, most wireless channels actually are not stationary where the received signals are fluctuated due to various factors. One of main factors that hinder the accurate prediction is the effects of human bodies [18]. Indoor wireless communications are more strongly influenced by human bodies because the antenna heights and the transmitted power are lower than those of outdoor systems.

Of the human bodies present in a wireless channel, a user is always located very close to a mobile device and affects the radio propagation on the wireless channel more strongly and consistently than other people. Therefore, it is meaningful that the effects of user body on wave propagation are

investigated exclusively separating from those of other human bodies. Moreover, considering the rapid growth in introduction of smart mobile devices, it is relevant to focus separately on the effects of user body.

Many studies on the influences of the human bodies including the user body have been reported. Researches which investigate the human body effects in the viewpoint of populations and moving patterns were reported [18-21]. Obayashi and Kaya [10] modeled the time-varying properties in populated channels with moving people using the combination of the ray-tracing and stochastic methods, whereas Kashiwagi [21] investigated those properties based on measurements. For the user body effects, authors in [19] and [20] investigated the changes in the radiation pattern and efficiency of the mobile antennas in the vicinity of an operator's body by using numerical methods and measurements. Lin and Chuang [22] evaluated the impact of the user body on the performance of a portable radio in urban mobile environments. Also, experimental analyses of user influence on MIMO channels were presented in [23], [24] and [25]. Particularly in regard to wireless body area networks (WBANs), many papers also investigated radio propagation taking into consideration the user body. Fort *et al*. [26] developed generic propagation models derived directly from Maxwell's equations for on-body channels. Cotton and Scanlon [27] also investigated on-body channels from the standpoint of user states with seven differently placed body-worn receivers. The authors presented that the Nakagami-*m* distribution best described on-body to on-body channels over all the measurement scenarios. For off-body channels, Koutitas [6] used a heuristic modified uniform theory

of diffraction (UTD) to analyze the on-body propagation due to the presence of a single or multiple bodies modeled as circular cylindrical surface and validated the results with the method of moment (MoM) and the measurements in an anechoic chamber.

1.3 Dissertation Outline

The remainder of this dissertation is organized as follows. In Chapter 2, the shadowing effects of user body on a single ray path are deterministically investigated based on the UTD. In Chapter 3, the application methodology of the UTD-based single ray model to multipath channel obtained by ray-tracing is proposed. Moreover, the statistical analysis of user body shadowing effects is also presented. Statistical properties for user body shadowing loss are characterized by ray-tracing simulation taking into consideration the randomness of the user's relative location. The shadowing loss model is established link-by-link with the Nakagami-*m* distribution and the estimated *m* parameters are presented as a function of K-factor. In Chapter 4, the improved user body shadowing models are proposed based on the bimodal characteristics of user body shadowing in links with high K-factor. Finally, conclusions were drawn in Chapter 5.

Chapter 2. User Body Shadowing Effects on Single Ray Path based on UTD

2.1 Introduction

In this dissertation, user body shadowing (UBS) effects on radio wave propagation are analyzed based on the UTD. At high frequencies, above 500 MHz, penetration of radio waves through a human body is insignificant, whereas waves diffracted on the surface of a human body are dominant field components [29]. So, the UTD is an appropriate and popular approach to investigate the effects of human bodies including users and pedestrians [28], [30]. Moreover, it provides deterministic ray-based solutions for various diffraction phenomena, which has an advantage of applicability with the ray-tracing technique.

In this chapter, the UBS effects on a single ray path are investigated deterministically by using the UTD. First of all, it is assumed that the position of user relative to incident direction of a ray with a receiver (user's device) as the center is the most significant factor to determine the UBS effects on the ray. Then, the received signal power is calculated according to the relative position of user with two different scenarios considering actual postures taken by the user using a mobile handset device. Additionally, the UTD-based analysis of the UBS effects on a single ray path is validated by measurements

in an anechoic chamber. In the anechoic chamber, the propagation environment is the same condition with the UTD analysis where the direct incident path exists only.

The remainder of this paper is organized as follows. In Section 2.2, a brief introduction of the UTD is presented. In Section 2.3, the solutions for diffraction at a smooth convex surface are explained. Because the user body can be modeled as a circular cylinder, the UTD solutions at a smooth convex surface are adopted. In Section 2.4, the UBS effects on a single ray path are characterized, and the validation results with anechoic chamber measurements are also presented. Finally, the main results are summarized in Section 2.5.

2.2 Uniform Theory of Diffraction (UTD)

To characterize deterministically the UBS effects, the UTD is adopted. The UTD is one of the popular methods which interpret the diffraction phenomena of radio wave. Under the high-frequency condition where the size of surrounding objects are larger than the order of a wavelength, the radio wave can be modeled as a ray and its propagation can be predicted by geometrical optics (GO). Although wave fields in the shadow region obstructed by an object are zero under the GO assumption, physical measurements indicate that the fields are not zero in reality. Historically, Keller presented the geometrical theory of diffraction (GTD) as the solution for diffraction by wedges in 1953 [31] and later expanded the principle to encompass diffraction by smooth

surfaces [32]. However, the original form of the GTD suffers from an accuracy problem near at shadow boundaries. It is because the asymptotic equation solutions of GTD change drastically in the vicinity of shadow boundaries. In mathematics, such a region in which equation solutions vary rapidly is called a boundary layer, and a solution valid even in the boundary layer is called a uniform solution. Kouyoumjian *et al.* developed the UTD valid in the proximity of shadow boundaries as the uniform solution of GTD [33], [34].

2.3 UTD Solutions for Diffraction at a Smooth Convex Surface

For the analysis of human body effect on wave propagation, diffraction at a smooth convex surface is considered because a human body can be modeled by a circular cylinder. The UTD distinguishes the phenomena of diffraction at a smooth convex surface into three different problems depending on the position of a source and an observation point [35]. When both the source and the observation point are off the surface, it is called the *scattering* problem; for the situation where either the source or the observation point is on the surface, it is referred to as the *radiation* problem; the case with both the source and the observation point on the surface is regarded as the *coupling* problem. Figure 2.1 shows these classifications of diffraction on a convex surface.

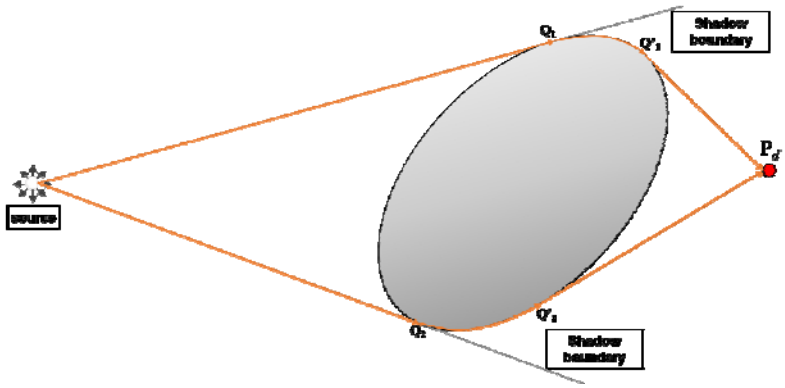

(a)

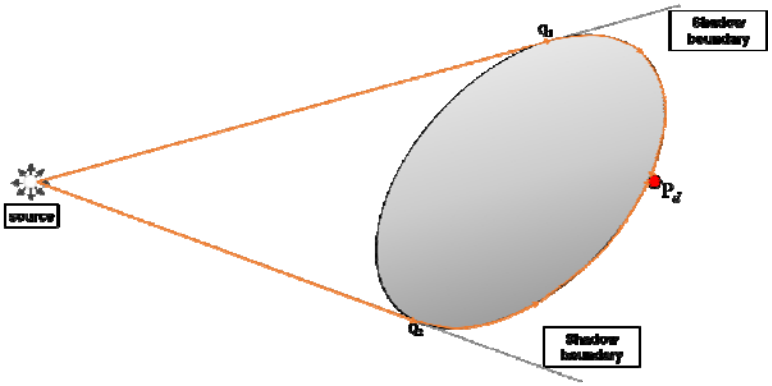

(b)

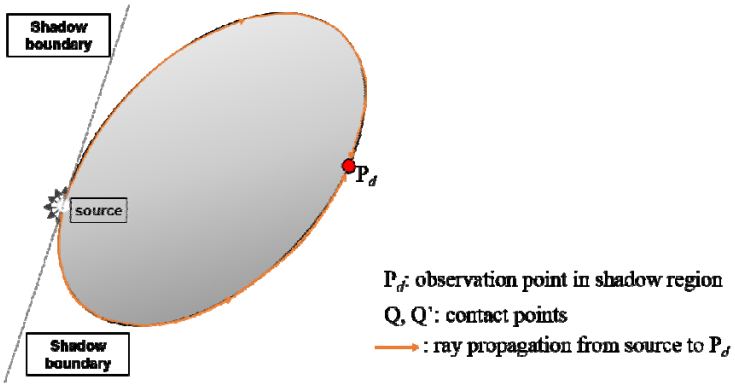

(c)

Figure 2.1 The classification of diffraction on a convex surface: (a) the scattering problems, the radiation problems, and (c) the coupling problem

In order to analyze the effects of a mobile handset user, both of the scattering problem and the radiation problem can be candidates considering the actual posture of the user. For example, the situation of voice communication is similar with the configuration of the radiation problem because the mobile device is adhered to the user's head. On the other hand, the scattering problem is more suitable to the situation of data communication where the device is held at a certain distance from the user's torso.

In this dissertation, the configuration of the scattering problem is adopted. According to [28], the UTD scattering solution with a simple heuristic modification can achieve good accuracy for the condition when the distance between the surface and the observation point is less than λ/4, where λ is the wavelength.

The UTD scattering solution is expressed differently in terms of the region in which the observation point is located. The related geometrical layout is shown in Figure 2.2. The total fields $U(P_l)$ and $U(P_d)$ in the lit and shadow region, respectively, are written as

$$U(P_l) = U^I + U^R = U^I + U^{IR} R_{s,h} A^R \tag{2.1}$$

$$U(P_d) = U^D = U^{ID} D_{s,h} A^D \tag{2.2}$$

where U^I is the direct incident field and U^R and U^D are the reflected and diffracted field, respectively; U^{IR} and U^{ID} are the incident field at the reflection and diffraction points, respectively; A^R and A^D represent the spreading factors after reflection and diffraction. U^{IR} and U^{IR} are the reflection and diffraction coefficients, respectively, and the subscripts represent the soft and hard case.

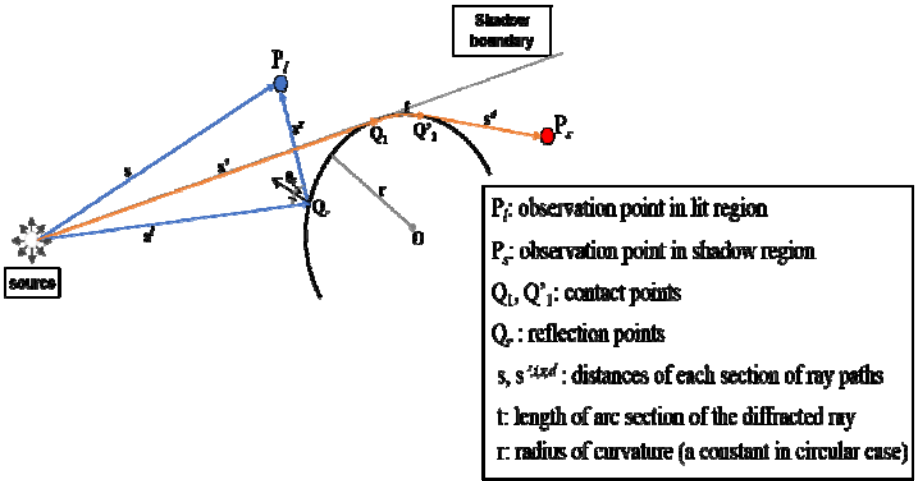

Figure 2.2 Geometrical layouts for the scattering problem

$$R_{s,h} = -\sqrt{\frac{-4}{\xi}} e^{-j(\xi)^3/12} \bullet \left\{ \frac{e^{-j\pi/4}}{2\xi\sqrt{\pi}} \left[1 - F(X) \right] + \begin{bmatrix} \hat{P}_s(\xi) \\ \hat{P}_h(\xi) \end{bmatrix} \right\} \qquad (2.3)$$

$$D_{s,h} = -m\sqrt{\frac{2}{k}} e^{-jkt} \bullet \left\{ \frac{e^{-j\pi/4}}{2\xi\sqrt{\pi}} \left[1 - F(X) \right] + \begin{bmatrix} \hat{P}_s(\xi) \\ \hat{P}_h(\xi) \end{bmatrix} \right\} \qquad (2.4)$$

where k is the wave number, and $F(X)$ and $\hat{P}_{s,h}(\xi)$ are the special functions called the transition function and the Pekeris caret function, respectively. The definitions of other parameters are presented in Table 2.1.

Table 2.1 Definitions of parameters for reflection and diffraction coefficients

Symbol	Definition	Equation for $R_{s,h}$	Equation for $D_{s,h}$
X	Argument of transition function $F(\bullet)$	$2kL\cos^2(\theta_i)$	$\frac{kL\xi^2}{2m^2}$
L	Distance parameter	$\frac{s^r s^i}{s^r + s^i}$	$\frac{s^d s'}{s^d + s'}$
ξ	Fock parameter	$-2m\cos\theta_i$	$\frac{mt}{r}$
m	Curvature parameter	$\left[\frac{kr}{2}\right]^{1/3}$	$\left[\frac{kr}{2}\right]^{1/3}$

A heuristic modification method is proposed in [36]. In original formula, the inaccurate cases are observed when the distance between the surface and the observation point is less than $\lambda/4$ and the observation point is in the deep shadow zone. This is because the transition function $F(X)$ does not approach 1 fast enough. Therefore, the term $F(X)$ is set by 1 manually when ξ is larger than 5 for the hard case and 2 for the soft case. This modification is validated for the case that the distance between the surface and the observation point is in the range of $\lambda/20$ to $\lambda/4$ [28]. Consequently, this condition is enough to satisfy the situation that the mobile device is almost adhered to the user body.

2.4 UBS effects on a Single Ray Path

As mentioned above subsection, the UBS effects on a single ray path are analyzed by the UTD scattering solution with a user body modeled as a circular cylinder. Above all, the shadowing angle θ is defined as the azimuth angle between the user's position and the incident direction of the direct propagation ray as shown in Figure 2.3. The shadowing angle θ determines whether the user blocks the ray path; the degree of blockage is the most important factor that decides the shadowing effects. Similar methods were introduced in WBANs for body-worn devices [28], however the present study focuses on the conventional portable handset devices that are kept at a certain distance from the user's body.

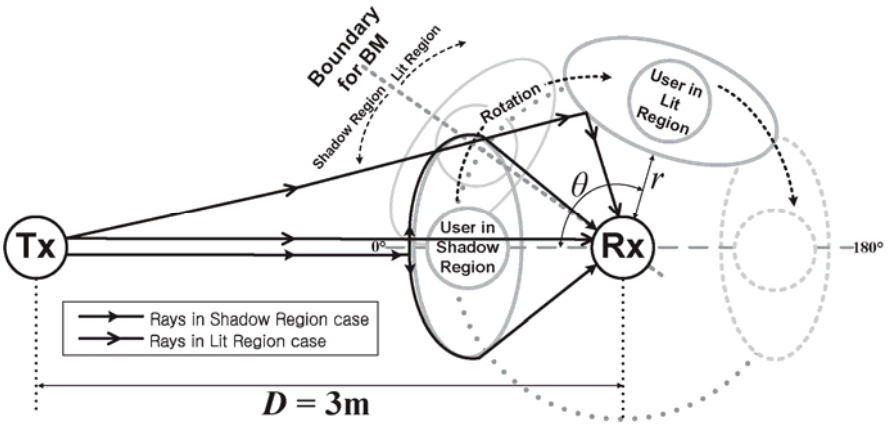

Figure 2.3 The top view of the modeling of UBS effects and the propagation mechanism of rays.

Additionaly, two different scenarios, namely the browsing mode (BM) and talking mode (TM), are considered to identify the effects of actual postures adopted when a person uses a mobile device. In UTD simulations, the user's torso for BM is modeled as a perfectly electric conducting (PEC) circular cylinder with a radius of 0.2 m, and the model of the user's head for TM is also defined as a circular cylinder of PEC material with a radius of 0.1 m. The distances separating the user from the receiver (r in Figure 2.3) are 15 cm and 2 cm, respectively. The signal powers relative to the reference power measured without the user are shown in Figure 2.4.

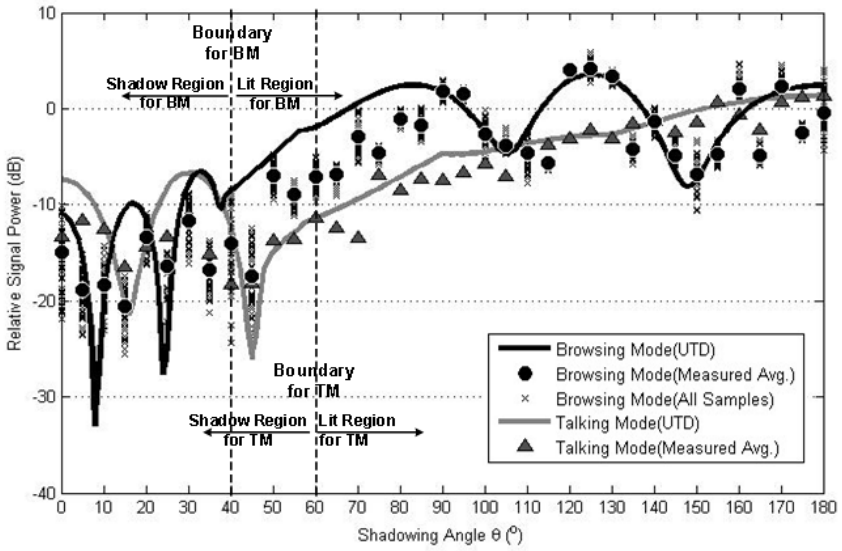

Figure 2.4 Comparison between the UTD scattering solution and the measurements in an anechoic chamber.

Measurements in an anechoic chamber were carried out for comparison with the UTD scattering solutions. The anechoic chamber of which size is 5 m × 10 m is at the Institute of New Media and Communications (INMC) of Seoul National University. The chamber and measurement system are shown in Figure 2.5 and Figure 2.6, respectively. A continuous wave (CW) at 2.4 GHz is generated by the signal generator (Agilent E8244A). The generated signal is amplified by the power amplifier with a gain of 30 dBm and radiated by the transmitted antenna. The transmitted signal is captured by the received antenna. Both antennas are the same omnidirectional antenna with 2 dBi gain. The received signal is amplified again by the low noise amplifier with a gain of 30 dBm. Finally, the power of received signal is measured by the spectrum analyzer (Agilent E4407B) and recorded into a laptop.

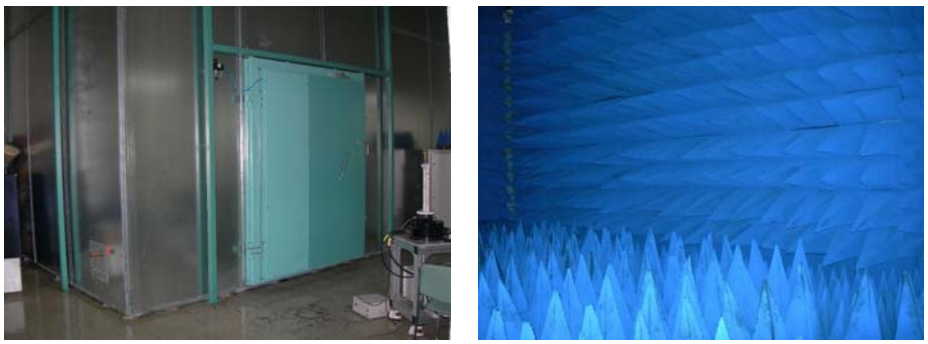

(a) (b)

Figure 2.5 Pictures of the anechoic chamber: (a) outside and (b) inside

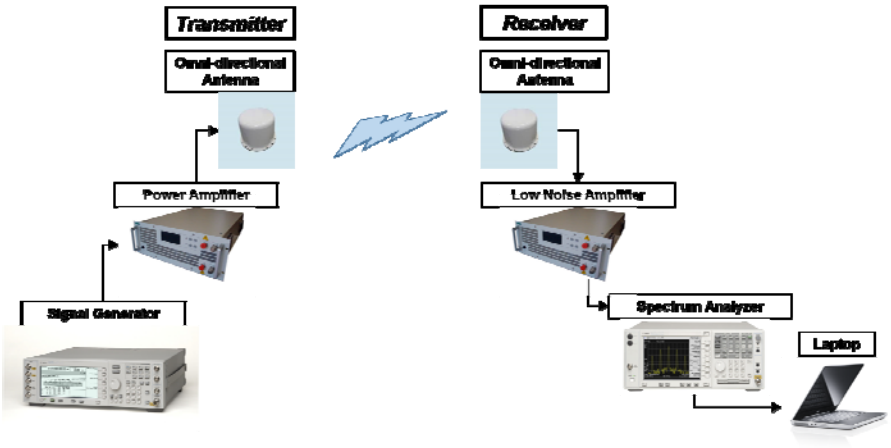

Figure 2.6 The CW measurement system

As in the UTD method, the distance between the transmitter and the receiver is fixed in 3 m. The received signal powers are measured as θ is changed from 0° to 180° with an increment of 10° by rotating the user around the receiver as shown in Figure 2.3. The transmitter is mounted on a tripod at a height of 1.25 m. On the other hand, the receiver is relocated at heights of 1.25 m (BM) and 1.6 m (TM), respectively. Further, the distance r is equal to that in the UTD simulations such as approxiamtely 15 cm (BM) and 2 cm (TM), respectively. Lastly, the test user is 1.7 m tall with a shoulder width of 0.45 m.

As shown in Figure 2.4, the measurement results and the UTD scattering solutions show fairly good agreement except for differences in fluctuation ranges in the shadow region. The fluctuation ranges of the UTD models are larger than those of the chamber measurements. In the UTD models, the distinct dips over 20 dB occur in the shadow region due to the phase

mismatch between two diffracted rays, whereas the fluctuation ranges in the chamber measurements are decreased to about 10 dB. Because the test user can not be perfectly fixed at an exact position during measurement process, the recorded signals at a shadowing angle vary as marked with '×' in Figure 2.4. Consequently, the averaging of those recorded samples smoothens the fluctuation ranges of shadowing loss based on the chamber measurements.

2.5 Conclusion

This chapter has analyzed deterministically on the UBS effects on single ray propagation by using the UTD scattering solutions. The shadowing angle θ was defined, which is the most significant parameter for determining the UBS. And then, the relative received signal power were calculated in terms of θ. Scenarios were divided into BM and TM depending on the user's posture.

The UTD-based models and the measurements in the anechoic chamber well coincide overall except for the gap between the fluctuation ranges in shadow region. On the basis of the UTD, the relative signal power shows the dips of 25–35 dB depending on the user's posture. In the measurements, however, the fluctuation range is reduced by about 10 dB due to averaging of the signals varied by minute movements of the test user.

Chapter 3. Analysis of UBS Effects on Indoor Wireless Multipath Channels

3.1 Introduction

The UBS effects on a single ray path has been modeled based on the UTD in the previous chapter. However, because practical indoor environments have multipath wirelss channels, the UTD-based models are necessary to be expanded for the multipath channels.

In this dissertation, the multipath information of indoor wireless propagation channels are obtained by ray-tracing technique. The ray-tracing is an efficient and reliable method to characterize site-specific channels such as indoor environments which have various structures and materials. Additionally, the ray-tracing provides not only received power of each path but also its angular profile. Because the UTD-based UBS model for a single ray path is established in terms of the shadowing angle θ, the angular profile of multipath fascilitate to simply combine the UTD-based model with the ray-tracing technique.

By using the combination of the UTD-based model and the ray-tracing technique, the UBS effects on indoor multipath channels are investigated deterministically depending on the fixed position of user. In realistic communications, however, the user's position can be neither fixed at any one value and nor can its exact value be provided to systems in real time. Thus, a

stochastic analysis that takes this randomness of the shadowing angle into consideration is required.

The remainder of this chapter is organized as follows. In Section 3.2, the ray-tracing technique utilized in this research is introduced. In Section 3.3, the application methodology of the UTD-based UBS model to multipath-angle profiles is proposed. In Section 3.4, the statistical analysis of UBS effects is presented. The conclusions are drawn in Section 3.5.

3.2 Ray-Tracing Technique

3.2.1 Image Method

A two-dimensional (2D) image-based ray-tracing technique is utilized in this study. Above all, 2D ray-tracing is appropriate as it takes into consideration UBS effects because the single ray path model based on UTD scattering solution uses the 2D shadowing angle θ as a parameter. The image method has relatively high computational complexity, but it is more accurate in terms of path-finding performance because there are no problems with missing or overlapping rays, in contrast to the shooting-and-bouncing ray (SBR) method [1]. Moreover, we improve the computational complexity by employing binary spatial partitioning (BSP) and beam-tracing techniques [37]. In the ray-tracing method, essentially, the propagation loss for each ray is calculated while including the free space loss and the additional factors stemming from multiple interactions with the surrounding objects. The received field strength E_i and the received signal power P_i for the ith

path can be written as

$$E_i = E_0\left(\frac{1}{2kd}\right)G_t G_r\left(\prod_{m=1}^{M}\rho_m\prod_{n=1}^{N}\tau_n\right)e^{-jkd} \tag{3.1}$$

$$P_i = |E_i|^2 \tag{3.2}$$

where k is the propagation constant and d is the unfolded distance of the path. G_t and G_r are the antenna gains of the transmitter and the receiver, respectively. ρ_m and τ_n are the m th reflection coefficient and n th transmission coefficient when M and N are the total number of reflections and transmissions, respectively. Thus, the local average power P_r at a receiver point is calculated from the sum of the powers of individual rays on a linear scale.

$$P_r = \sum_i P_i = \sum_i |E_i|^2 \tag{3.3}$$

3.2.2 Reliability

The reliability of the 2D ray-tracing technique is validated by a comparison with in-building measurements. The measurements were taken in the basement of a laboratory building. As shown in Figure 3.1, the scenarios were divided into two cases depending on the position of the transmitter. The transmitter was located in the seminar room (TR) or in the corridor (TC), and the receiver positions were classified as the LOS and NLOS cases. As a result, four and ten LOS links were selected for TR and TC, respectively, whereas eight and twelve NLOS links were chosen for each scenario. Both the seminar

room and the athletic room were typical open rooms devoid of furniture except for several concrete pillars. The corridor was narrow with a width of approximately 2 m.

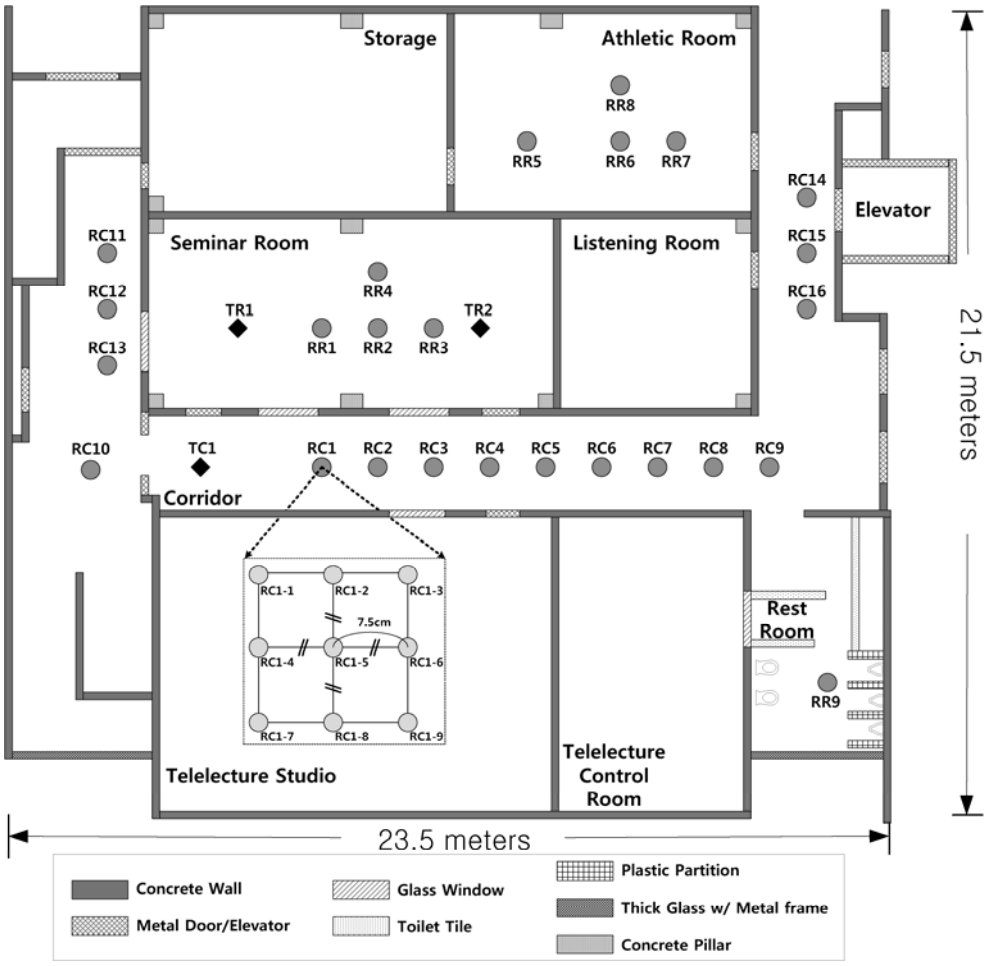

Figure 3.1 Layouts of the measurement site, the basement of laboratory building.

For the channel measurements, small-scale fading needs to be canceled out to obtain reliable local average power at the receiver point. Therefore, as shown in Figure 3.1, as the enlarged part of RC1, the received signal powers around nine local points approximately 7.5 cm (0.6 λ) away from the receiver point were measured. 100 data samples were recorded per measurement, with a total of 900 samples therefore obtained per receiver point. The local mean power was then calculated by averaging these values. The transmitted signal power was 10 dBm at 2.4 GHz. The transmitter and receiver were the same omnidirectional antennas used in the anechoic chamber measurements, and both were mounted on tripods at a height of 1.25 m. The comparison results of the ray-tracing predictions and the in-building measurements are presented specifically in Table 3.1 and 3.2. As shown in the table, the predictions show good accuracy, with error statistics of 1-2 dB on average with standard deviations in a range of 3-5 dB.

Table 3.1 Comparison of Ray-Tracing and Measurements for LOS cases

TX	TR1				TC1			
Link	RX	CW Measure (dBm)	Ray Tracing (dBm)	Error (dB)	RX	CW Measure (dBm)	Ray Tracing (dBm)	Error (dB)
LOS					RC1	-44.18	-40.45	3.73
					RC2	-41.33	-42.38	-1.05
					RC3	-43.78	-44.40	-0.62
	RR1	-34.64	-38.27	-3.63	RC4	-45.91	-45.57	0.34
	RR2	-40.18	-41.75	-1.57	RC5	-42.38	-44.86	-2.48
	RR3	-44.86	-44.24	0.62	RC6	-46.43	-46.17	0.26
	RR4	-38.91	-42.07	-3.16	RC7	-49.81	-46.96	2.85
					RC8	-48.67	-47.74	0.93
					RC9	-53.07	-46.56	6.51
					RC10	-39.24	-41.94	-2.70
	Error Statistics		Avg. Stdev.	**-1.94** **1.918**	Error Statistics		Avg. Stdev.	**0.78** **2.874**

Table 3.2 Comparison of Ray-Tracing and Measurements for NLOS cases

TX	TR1				TC1			
Link	RX	CW Measure (dBm)	Ray Tracing (dBm)	Error (dB)	RX	CW Measure (dBm)	Ray Tracing (dBm)	Error (dB)
NLOS					RR1	-50.75	-46.01	4.74
					RR2	-56.27	-48.07	8.20
	RR5	-70.99	-73.86	-2.87	RR3	-56.54	-51.13	5.41
	RR6	-67.42	-71.81	-4.39	RR6	-78.46	-72.80	5.66
	RR7	-72.63	-78.55	-5.92	RR7	-75.57	-71.10	4.47
	RR8	-68.02	-69.40	-1.38	RR9	-80.99	-83.01	-2.02
	RC1	-52.42	-48.16	4.26	RC11	-55.71	-54.12	1.59
	RC2	-57.09	-58.13	-1.04	RC12	-53.41	-46.68	6.73
	RC3	-58.49	-61.60	-3.11	RC13	-49.89	-52.92	-3.03
	RC4	-56.88	-54.55	2.33	RC14	-69.66	-73.62	-3.96
					RC15	-64.40	-72.29	-7.89
					RC16	-62.82	-67.72	-4.90
	Error Statistics		Avg. Stdev.	**-1.52** **3.390**	Error Statistics		Avg. Stdev.	**1.25** **5.354**

3.3 Application of the Single Ray UBS Model to Multipath Channel

3.3.1 Methodology

In this subsection, the combining method of the multipath channel profile obtained by ray-tracing and the UTD-based single ray UBS model is proposed. Since the UBS model for a single ray path is established as a relation between the shadowing angle θ and the relative power loss in decibels, it can be simply applied to multipath angle profiles of ray-tracing simulations as an additive power loss to each path. It can be expressed as

$$P_i^{\mathrm{UBS}}(\theta_i) = P_i - L^{\mathrm{UBS}}(\theta_i) \quad [\mathrm{dB}] \tag{3.4}$$

where $P_i^{\mathrm{UBS}}(\theta_i)$ is the received signal power of the ith path when it undergoes user shadowing, and θ_i and $L^{\mathrm{UBS}}(\theta_i)$ are the corresponding shadowing angle and UBS loss, respectively. As shown in Figure 3.2, each shadowing angle θ_i is determined by the relation between the user's position α and the arrival angle of the ith ray path β_i. Additionally, look-up tables are constructed with the UTD-based models in the angle range from 0° to 180° at intervals of 0.1°, and the actual value of shadowing loss is obtained by the linear interpolation. Finally, the total received power P_r^{UBS} in decibels can be calculated as

$$P_r^{\mathrm{UBS}} = 10\log_{10}\sum_i 10^{P_i^{\mathrm{UBS}}(\theta_i)/10} \quad [\mathrm{dB}] \tag{3.5}$$

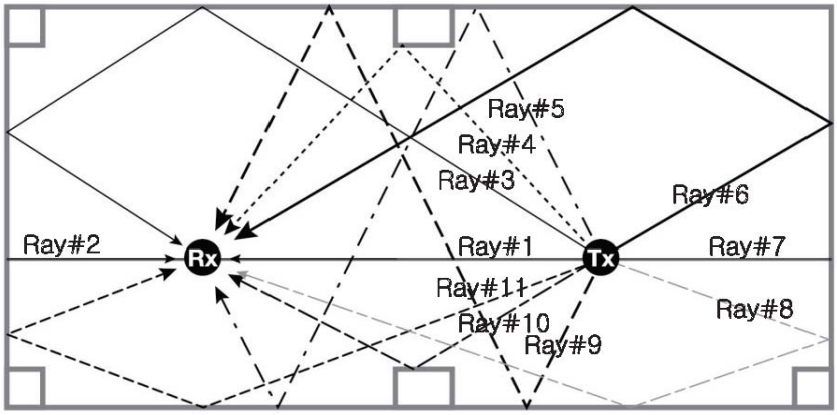

(a)

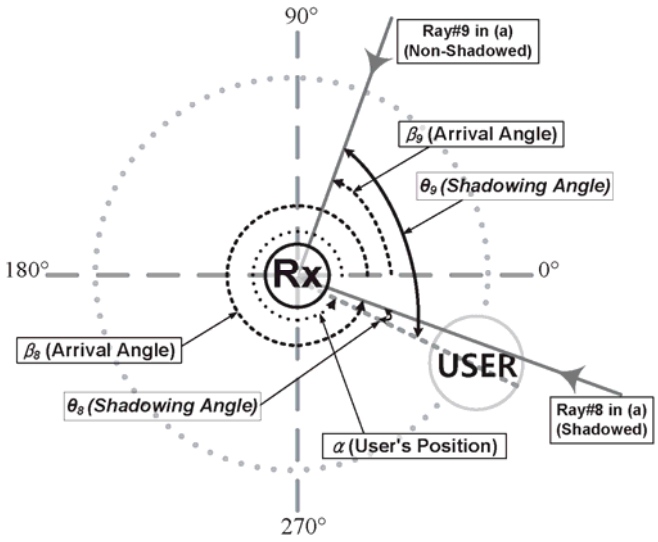

(b)

Figure 3.2 (a) All traced rays on a link in an open room (b) Shadowing angles of two representative rays depending on the arrival angles of the rays and the user's position.

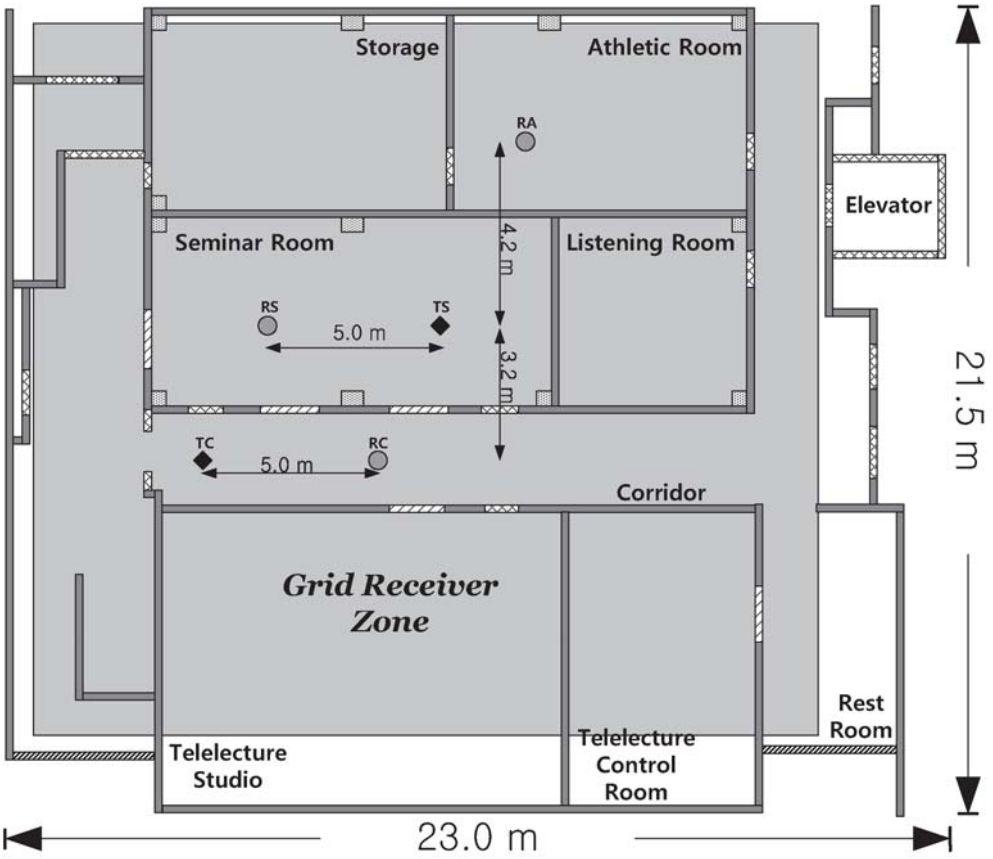

Figure 3.3 Geometrical layout of the measurement building and the transmitter/receiver positions.

3.3.2 Validation

The ray-tracing predictions taking the UBS effects into consideration are also validated by comparison with the measurements. As shown in Figure 3.3, four different transmitter-receiver pairs such as two LOS (TS-RS, TC-RC) and two NLOS (TS-RA, TS-RC) were chosen. Both the seminar room and the athletic room were emptied of furniture except for several concrete pillars and the corridor was about 2 m wide. Both the transmitter and the receiver were equipped with omnidirectional antennas mounted on tripods at the height of 1.25 m. The transmitted signal power was 10 dBm at 2.4 GHz, and the received powers were measured with a test user who rotated 360° in increments of 10°. The user state was assumed to be BM. 100 of received signal powers were recorded at each user angle for a given transmitter-receiver pair, so 3600 samples of received signal powers were collected for the entire shadowing angle. The same measurement process was repeated four times for the same pair. Consequently, 14,400 data samples were obtained for one scenario, and the averages of 400 samples for each shadowing angle are compared to the ray-tracing predictions in Figure 3.4.

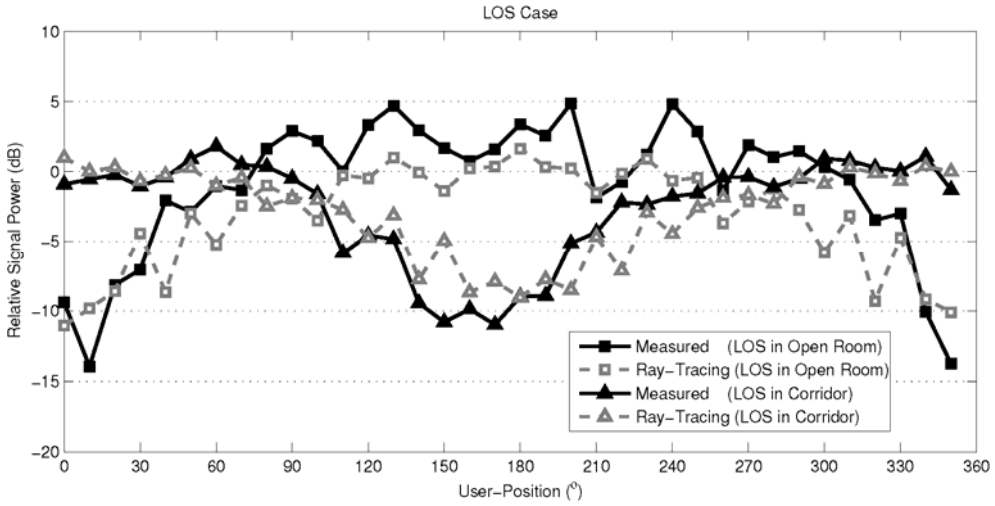

(a)

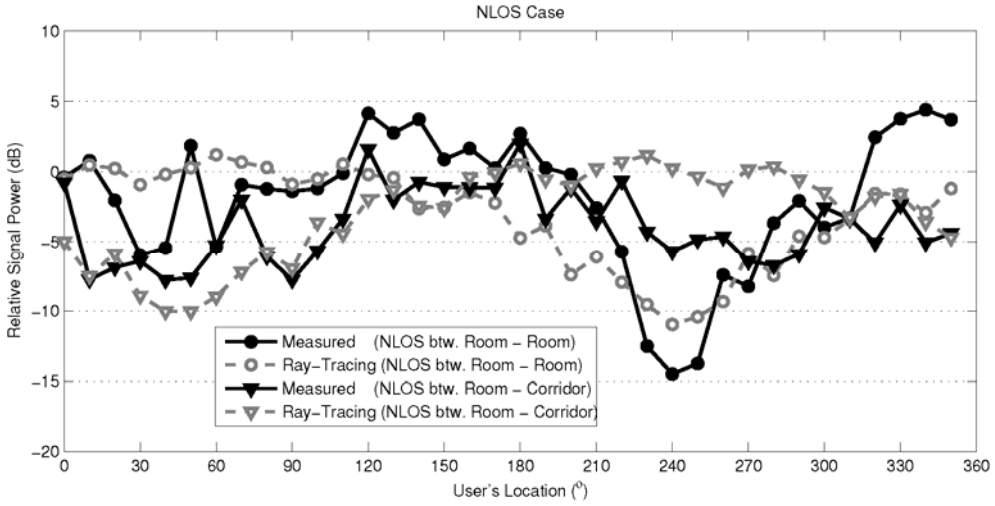

(b)

Figure 3.4 Comparison of the ray-tracing predictions taking user shadowing into consideration with the in-building measurements: (a) LOS (b) NLOS

In both LOS and NLOS cases, the ray-tracing predictions agree fairly well with the measurement results. Since the directions of the direct path are evident for LOS cases (0° in TS-RS, 180° in TC-RC), the shadowing loss is increased up to about 14 dB and 11 dB, respectively when the user is located near those directions. In the similar manner, for NLOS cases, there might be relatively dominant paths in the multipath environment. Therefore, it can be expected that the large shadowing loss occurs when these dominant paths are obstructed by the user. In the results in Figure 3.4(b), the direct paths can be thought of as the dominant paths even in NLOS (about 240° in TS-RA, 45° in TS-RC), because the nearby user's positions experience more losses in received power than others.

3.4 Link-by-Link Model using Nakagami-*m* Distribution

As explained in the previous section, the UBS effects change according to the extent of the dominant signal in multipath channels. Therefore, the K-factor, defined as the ratio of the power in the dominant path and the sum of the powers in the other paths, can be an appropriate indicator of the magnitude of the UBS effects. Moreover, since the discrete channel impulse responses are obtained by ray tracing, the K-factor for each channel link can be simply calculated as the ratio of the strongest ray's power to the sum of the powers of the other rays.

First, sufficient numbers of links were settled for the simulations. Receiver grids were placed 1 m apart in the gray-colored simulation zone of size 20 m × 20 m as shown in Figure 3.3. Two transmitter positions, TS and TC, were used again. The simulation zone covers most region in which mobile devices can be located in the measurement site. Except for the receiver positions that overlaps with the transmitters, a total of 798 links (399 grid receivers × 2 transmitters) are selected including both LOS and NLOS. The statistics of UBS effects change in terms of user's positions and multipath characteristics. The multipath characteristics of each link are obtained deterministically from the ray-tracing simulation, whereas the user's positions are generated from 0° to 360° at intervals of 0.1° under the uniform distribution assumption. Consequently, the random variable of total UBS loss $L_{\text{tot}}^{\text{UBS}}$ in decibels is defined as

$$L_{\text{tot}}^{\text{UBS}} = P_r^{\text{UBS}} - P_r \quad [\text{dB}] \tag{3.6}$$

where P_r^{UBS} is the received power that takes UBS effects into consideration and P_r is the received power without UBS effects.

For a statistical model, the Nakagami-*m* distribution is considered. The parameters of the Nakagami-*m* distribution, m and Ω, are obtained by maximum likelihood estimation on a 95% confidence interval using the library function in Matlab. The Nakagami-*m* distribution, one of the probability distributions that has been used to model the fading effects in wireless multipath channels [38], [39], is represented by the probability

density function (PDF)

$$p(x;m,\Omega)=\frac{2}{\Gamma(m)}\left(\frac{m}{\Omega}\right)^{m}\times x^{2m-1}\exp\left(-\frac{m}{\Omega}x^{2}\right) \qquad (3.7)$$

$$for\ x\geq 0, m\geq 0.5, \Omega\geq 0$$

where x is the random variable, and $\Gamma(\cdot)$ is the gamma function.

The scattered markers in Figure 3.5 represent estimated m of 798 links on the basis of total UBS loss distribution according to the uniformly generated random user's positions. The regression curve between the K-factor and the estimated m is also indicated with a solid line in Figure 3.5. In case of Ω, the estimated values vary relatively independent of the K-factor in both modes. The averages of Ω are 0.68 and 0.46 in BM and TM, respectively. The Kolmogrov-Smirnov (K-S) test is performed as a goodness-of-fit test to verify how well the Nakagami-*m* distribution fits the distribution of the total UBS loss. The statistic of K-S test which means the maximum difference between the empirical cumulative distribution function (CDF) and the theoretical CDF of a candidate distribution. The K-S test is conducted for each total UBS loss distribution of 798 links with four conventional probability distributions such as the Nakagami-*m*, Rician, Gaussian, and Rayleigh distributions. The results are shown in Table 3.3. The K-S test statistics for the mean and minmum values have marginal difference between the Nakagami-*m*, Rician, and Gaussian distributions. However, for the maximum value which indicates the worst fit case, the Nakagami-*m* distribution is far superior to the others.

Table 3.3 K-S test statistics of the candidate distributions

Candidate	K-S Test Statistic		
	Mean	Min.	Max.
Nakagami-*m*	**0.0996**	**0.0289**	**0.1376**
Rician	0.1109	0.0274	0.1956
Gaussian	0.1015	0.0247	0.1830
Rayleigh	0.1362	0.0415	0.3599

The estimated Ω of BM is lower than that of TM, because the probability that a mobile device is in the shadow region is lower owing to the greater distance between the mobile device and the body for BM. As shown in Figure 3.5, on the other hand, m shows an exponentially decreasing tendency as the K-factor increases. According to [39], the change of m results from an increase in variation of user-shadowing loss because the variation is the denominator of m where the numerator equal to the square of Ω, which is independent of the K-factor. The large variation of user-shadowing loss in high K-factor, as we expected, supports the notion that the extent of the dominant signal has a crucial effect on instantaneous user shadowing.

In addition, to elaborate the statistical model for m, we notice the dispersive patterns of the estimated m values centering around the regression lines as shown in Figure 3.5. The m values coincide very well with the regression curve when K-factors are large, but are more dispersive for small K-factors. A small K-factor, which means that a dominant path is weak, implies that whether the path is shadowed becomes less important than

other factors such as density and angular spread of the multipath. Consequently, we propose modified statistical models for the Nakagami-*m* parameter as the sum of the regression function and random variables of zero-mean Gaussian distributions with standard deviations that depend on the K-factor. The specific results are summarized in Table 3.4.

Table 3.4 Nakagami-*m* parameters for statistical UBS models

Mode	m	Ω	Expected Range of K-factor
BM	$2.758\exp\left(-0.171K\right)+0.760+N\left(0,\sigma_{m,\mathrm{BM}}^2\right)$ $\sigma_{m,\mathrm{BM}}=0.530\exp\left(-0.1857K\right)$	0.68	-7 dB $\le K \le$ 20 dB
TM	$1.709\exp\left(-0.293K\right)+1.308+N\left(0,\sigma_{m,\mathrm{TM}}^2\right)$ $\sigma_{m,\mathrm{TM}}=0.686\exp\left(-0.2536K\right)$	0.46	

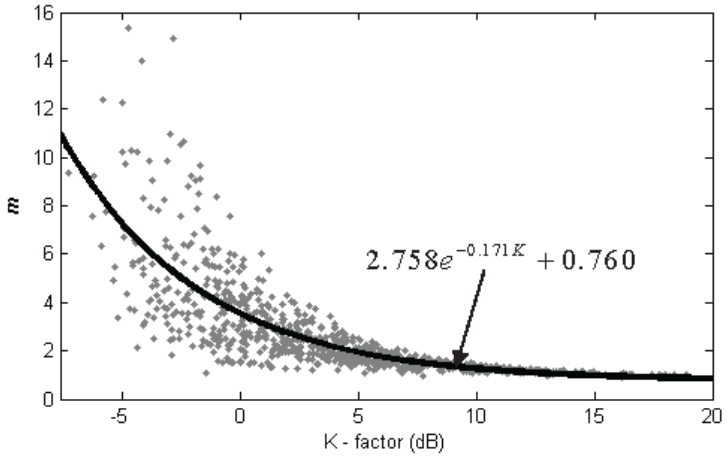

(a)

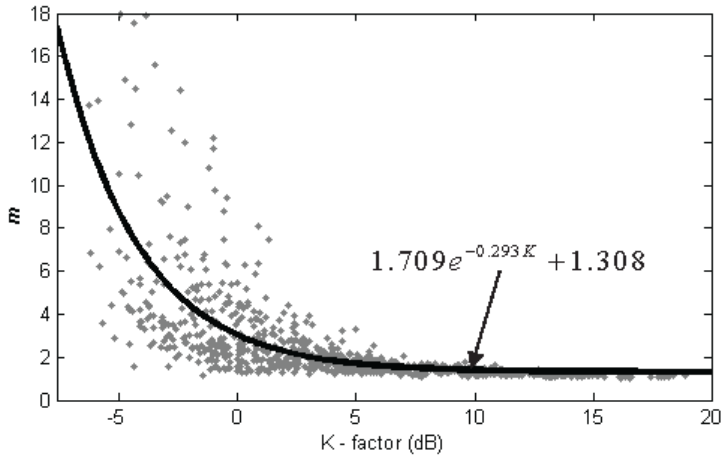

(b)

Figure 3.5 Relations between Nakagami-*m* parameters and K-factors for (a) BM and (b) TM.

3.5 Conclusion

Applying this single path shadowing model to multipath channels obtained by the ray tracing. The ray-tracing technique is an efficient method of obtaining site-specific channel information. It provides reliable predictions for stationary channels in which both the transmitters and receivers are fixed. The error statistics showing a 1 dB average and a 4 dB standard deviation are estimated in a comparison with in-building measurements. Finally, the ray-tracing predictions taking into consideration the UBS effects were also validated with in-building measurements. In the ray-tracing predictions, the signal variations depending on the shadowing angle coincide very well with the measurements. For further works, the statistical characteristics of the UBS effects taking into consideration the randomness of the shadowing angle need to be analyzed, because the shadowing angle can neither be fixed at any one value and nor can its exact value be provided to systems in real time.

Chapter 4. Enhanced Statistical Model for UBS based on Bimodal Characteristics

4.1 Introduction

In the previous chapter, the deterministic and statistical UBS models for indoor wireless channel has been proposed which works based on ray-tracing simulation combined with the UTD [40]. The modeling procedure described in Chapter 2 and Chapter 3 is summarized in three steps as follows: first, the UBS effect on a single ray path is modeled as the relationship between the user's position and the relative signal losses based on the UTD, and the result is validated by measurements in an anechoic chamber. Second, the UBS model on a single path is applied to multipath-angle profiles of indoor wireless channel obtained by ray-tracing simulation, and the result is also verified using in-building measurements. Finally, the UBS effect is statistically analyzed by considering the randomness of the user's relative position to the receiver.

As a result, the distributions of the total UBS losses for 798 links are modeled by using Nakagami-*m* distributions. In particular, the parameters of the Nakagami-*m* distribution are expressed as a function of K-factor. The Nakagami-*m* distribution is selected based on the K-S test statistics as mentioned in the previous chapter. However, as shown in Figure 4.1, the measure of K-S test, defined as the maximum difference between CDFs of the

empirical data and the Nakagami-*m* CDF, is larger in the links with high K-factor. This means that the fitting accuracy gets worse along with increasing K-factor.

In this chapter, the improved UBS models are proposed to overcome the drawback of accuracy in the previous model. First of all, we notice that the distributions of the total UBS losses of links with high K-factor appear in bimodal shape that has two peaks in its PDF. The physical reason of the bimodal characteristic and the relationship between K-factor of links and the bimodal characteristic are explored. Then, links are grouped in accordance with the modality of the distributions for achieving simplicity and representativeness of the enhanced model in this chapter. Finally, the new UBS models are established for each group. In addition, two minor factors are also considered in this model: the distance between the user and the receiver and the radius of the user modeled as a cylindrical body. They were fixed in the previous model because variations in them cause less significant effect on the determination of the UBS effect than the changes in the user's position. However, since they demonstrate randomness definitely in the practical situation, we define them as random variables in the evaluation of the accuracy of the newly proposed model.

The remainder of this chapter is organized as follow. In Section 4.2, we explain our methodology used to elaborate the enhanced UBS models. In Section 4.3, a setup of ray-tracing simulation is detailed. In Section 4.4, the improved UBS models are proposed and their applicability to various

environments is addressed. Last, our results are summarized, and some future works are discussed in Section 4.5.

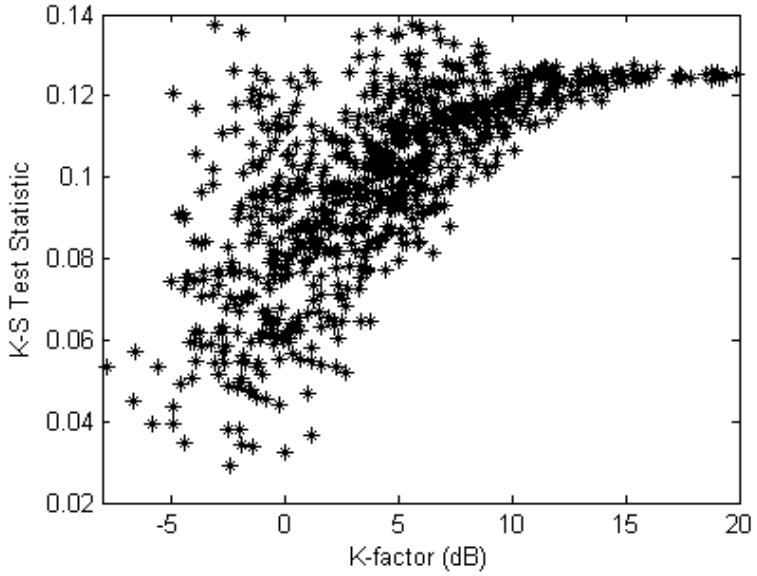

Figure 4.1 Change of K-S test statistics in terms of K-factor

4.2 Methodology for Enhancement of UBS Model

In the previous chapter, the total UBS loss L_{tot}^{UBS}, which is a dimensionless value, is defined as

$$L_{tot}^{UBS} = P_r^{UBS} / P_r \tag{4.1}$$

where P_r^{UBS} is the received power that takes the UBS effect into consideration, and P_r is the received power without the UBS effect, both of which are expressed in watts. Moreover, the distributions of the total UBS losses, which we also refer to as the UBS distributions hereafter, are fitted to the Nakagami-*m* distribution. As mentioned in the previous chapter, the Nakagami-*m* distribution is selected using K-S test, but the statistic of K-S test gets larger along with the increasing K-factor. Actually, we graphically confirmed the precision of distribution fitting and typical examples are shown in Figure 4.2 and 4.3. The figures are sorted in ascending order of K-factor. As shown in Figure 4.2 and 4.3, the UBS distribution for the link with low K-factor has a unimodal characteristic, which is in good agreement with the Nakagami-*m* distribution for both scenarios. In contrast, when K-factor of link is higher, the UBS distributions have evidently more different shapes from the existing well-known distributions including Nakagami-*m* distribution. These imply that the statistic of K-S test can provide a relative preference among the candidate distributions, but it is not appropriate to decide the absolute precision [41]. In this section, we figure out this feature, which we overlooked

in the previous model [40], and propose the methodology to improve the UBS model.

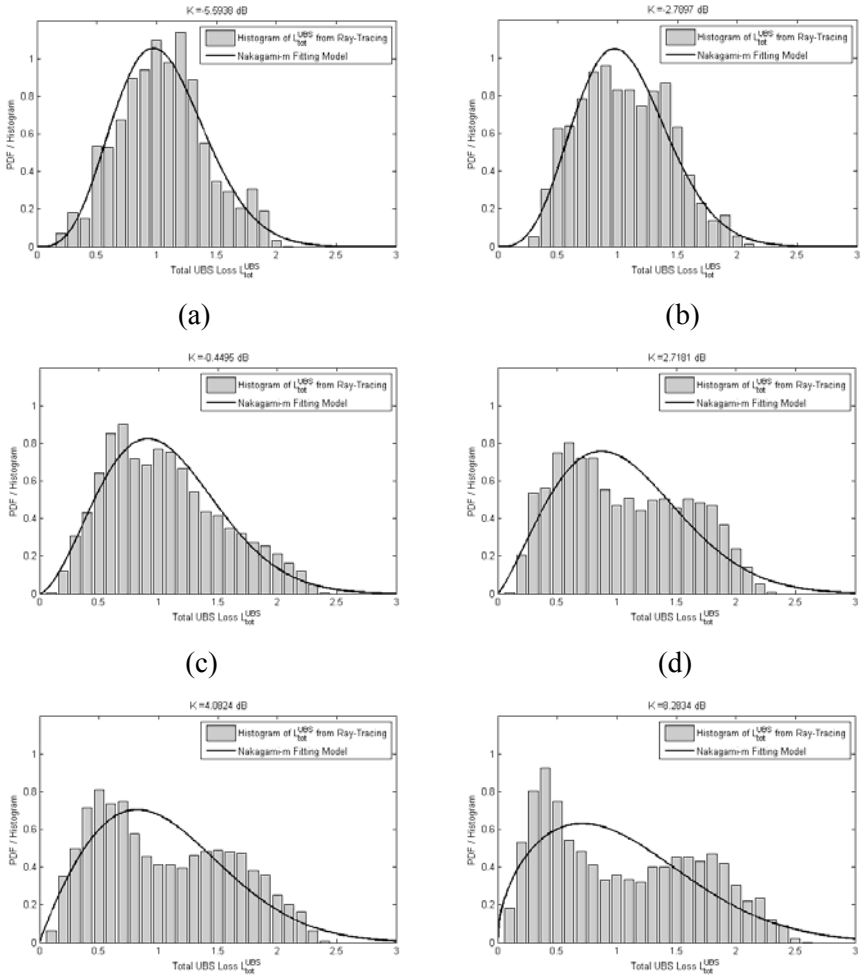

Figure 4.2 Nakagami-*m* fits for BM with increasing K-factor of links

(a) -5.59 dB, (b) -2.79 dB, (c) 0.45 dB, (d) 2.72 dB, (e) 4.08 dB, (f) 8.28 dB

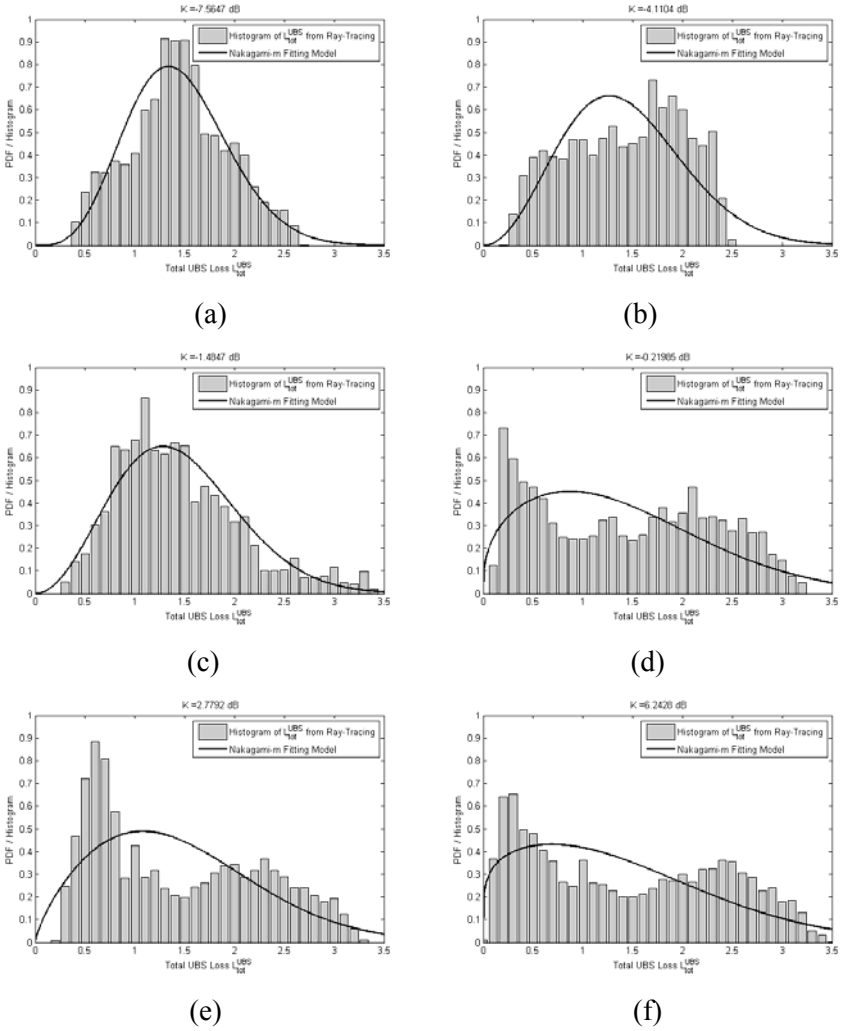

Figure 4.3 Nakagami-*m* fits for TM with increasing K-factor of links

(a) -7.56 dB, (b) -4.11dB, (c) -1.48 dB, (d) 0.22 dB, (e) 2.78 dB, (f) 6.24 dB

4.2.1 Bimodal Characteristics of the UBS Model

As shown in Figure 4.2 and 4.3, the distribution of the total UBS losses for the link with high K-factor shows the bimodal characteristic. The physical reason for this bimodal UBS distribution can be understood by the definition of K-factor. High K-factor means that the most dominant path exists distinctly in a link, which also means that the UBS effect is mainly depends on whether the most dominant path is shadowed by the user. Consequently, the UBS distribution in the link with high K-factor appears as a sum of two different characteristics regarding whether the most dominant path is obstructed. On the other hand, when a link has lower K-factor, the UBS distribution is closer to a unimodal one. In a similar way, low K-factor means that there is no evident dominant path by which the UBS effect is determined.

For a quantitative criterion to classify the UBS distributions into unimodal and bimodal ones, we adopt Sarle's bimodality coefficient (BC) [42]. BC is defined empirically as a relationship between bimodality and the third and fourth standardized moments of the distribution so called *skewness* and *kurtosis*, respectively. The skewness is a measure of asymmetry of a probability distribution about its mean. For a unimodal distribution, the skewness has either a negative or a positive value depending on whether the data distribution is skewed either to the left or to the right of the mean, and its value is zero for a symmetric distribution. On the other hand, the kurtosis is a measure of spikiness of a distribution. A distribution with a sharper peak and fatter tails than the normal distribution has a high kurtosis value, whereas a distribution with a more rounded peak and thinner tails has a low kurtosis. BC

is defined in terms of the skewness s and the kurtosis k as follows.

$$BC = \frac{s^2 + 1}{k} \tag{4.2}$$

This definition is interpreted with the intuitive logic that a bimodal distribution will be close to a more rounded peak than a unimodal distribution (low k) and have an asymmetric feature (high s^2), which results in the increased BC value. BC has values ranging from 0 to 1. When BC exceeds 0.555, it implies that the distribution is close to a bimodal one because the value of 0.555 represents the worst case of unimodal distribution, i.e., the uniform distribution.

4.2.2 Data Grouping

The previous model was established based on the link by link estimated Nakagami-*m* parameters. It is quite complicated to use this model because different m values should be generated for each link as Gaussian random variables with both mean and standard deviation vary with K-factor. In this chapter, however, the links are classified into a unimodal and a bimodal group, and the distribution model of the total UBS losses for each group is proposed. The models formulated by grouping provide the advantage of simplicity and reusability. This approach is similar to the log-normal shadowing model for distance-based path loss [1]. In this model, the received signals at points that are in the same distance from the transmitter are collected, and a normal distribution on a log scale is observed for the variation of those signals. The distance between the transmitter and the receiver is the main indicator of the

distance-based path loss model, whereas the K-factor is that of the UBS model, which was suggested in [40]. Total UBS losses for links with K-factors less than a threshold are collected, and their variation is found to follow a unimodal distribution. Similarly, collecting the total UBS losses for links with K-factors higher than the threshold, a bimodal model is suggested to describe their variation. More details are dealt with in Section 4.4.

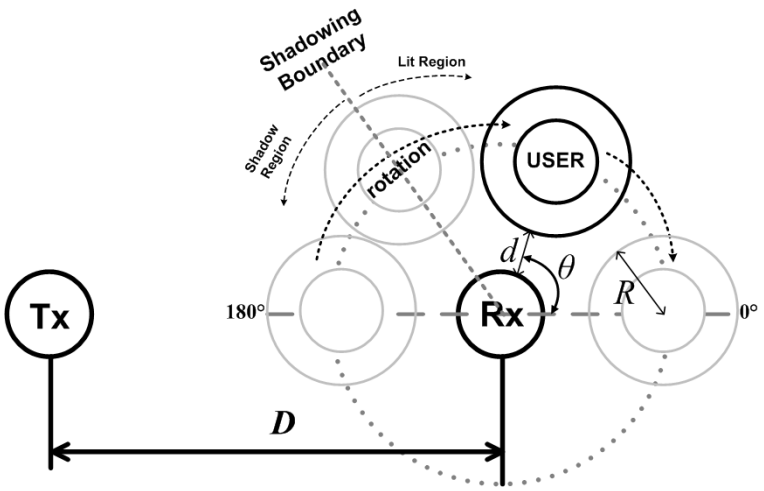

Figure 4.4 Modeling concept of the single path UBS model.

4.2.3 Other Factors

In enhanced UBS model, two additional factors are also considered in the UTD-based single ray model. The first one is the distance between the user and the receiver, and the second is the radius of the user modeled as a circular cylinder. They are denoted as d and R, respectively, in Figure 4.4 which is the conceptual image of UBS modeling for a single ray path. In Chapter 2 and Chapter 3, both these factors are fixed at the typical values because the effects of them are much less significant than the those of the shadowing angle θ. As shown in Figure 4.5 and 4.6, however, changes of these two factors affect slightly, but distinctly the single path UBS model based on the UTD. Therefore, it is assumed that both the factors are uniformly distributed random variables at appropriate intervals considering the practical situation and the reliability of UTD scattering solution. Specifically, the interval of d is from 0.1 m to 0.3 m and the radius R ranges from 0.18 m to 0.25 m in BM scenario. On the other hand, the interval of d is from 0.01 m to 0.03 m and the radius R ranges from 0.08 m to 0.12 m for TM scenario. Those had the fixed values $\{d = 0.15$ m, $R = 0.2$ m$\}$ and $\{d = 0.02$ m, $R = 0.1$ m$\}$ for BM and TM, respectively, in the previous model. Consequently, the UTD-based signal loss due to the UBS is finally determined based on the values of the shadowing angle θ, the receiving antenna distance d, and the radius R.

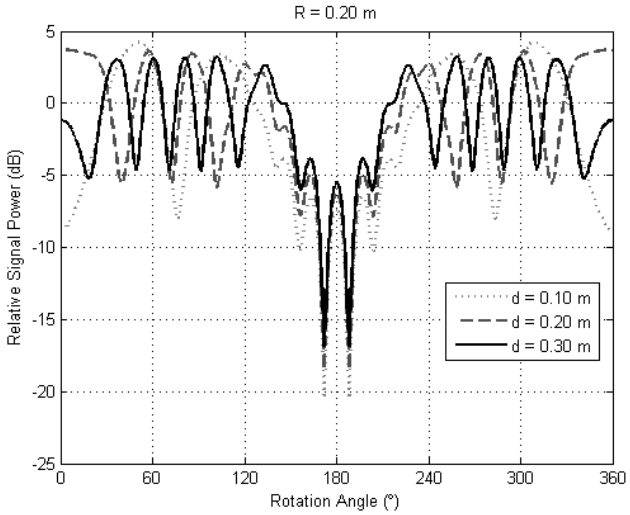

(a)

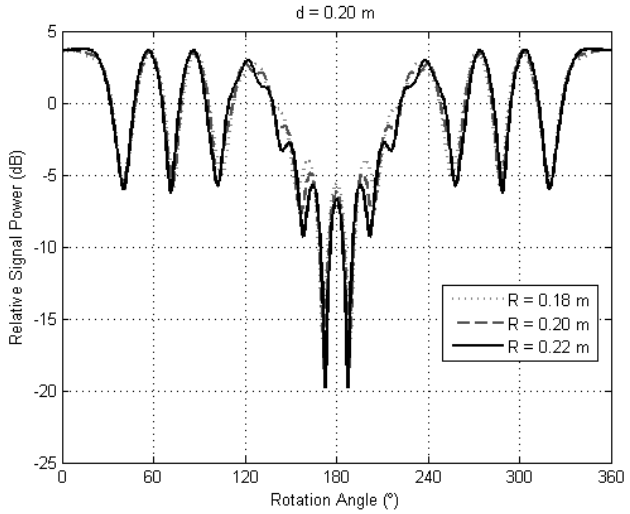

(b)

Figure 4.5 Effects of variation of (a) d and (b) R for BM

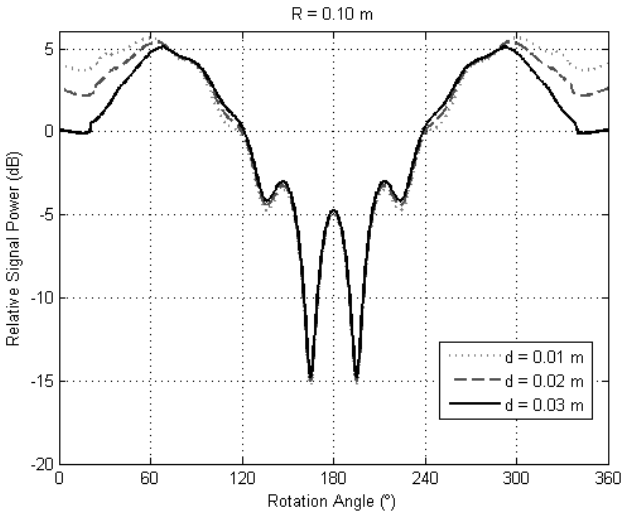

(a)

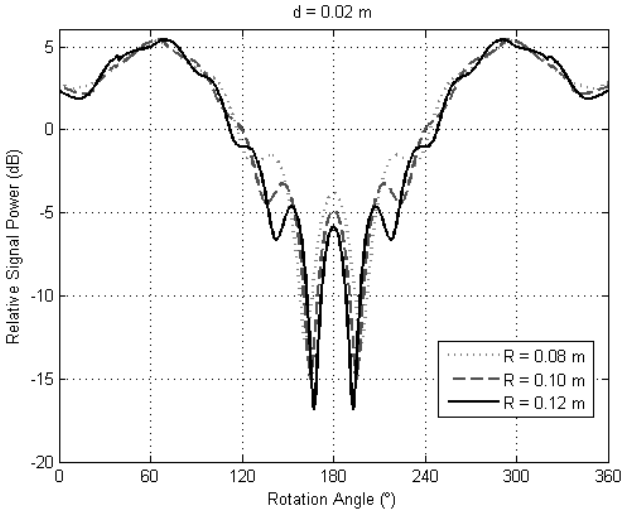

(b)

Figure 4.6 Effects of variation of (a) d and (b) R for TM

4.3 Ray-Tracing Simulation

Ray-tracing simulation is conducted to get the data of the total UBS losses at the same environment proposed in Chapter 3, which is a typical laboratory building. The floor plan is shown in Figure 4.7. There are three transmitter points and gray rectangles named ‘RX Grid Zone’ representing the grids of receiver points. Unlike the setup in Chapter 3, the area of receiver grid is adjusted considering the practical location of the user device. Additonally, for reliability of new proposed model, simulation links are divided into training and test groups to conduct the 2-fold cross-validation. Totally 263 links are set as the training group in the ‘RX Grid Zone’ 1 to 4, whereas 240 links are set as the test group in the ‘RX Grid Zone’ 5 to 8, without distinction between LOS and NLOS. Consequently, the parameters of distribution models are estimated based on data from the training group and the fitness is visually confirmed with data from the test group.

Ray-tracing technique utilized in this paper is based on image method that accommodates the number of reflections for each ray propagation up to five. The maximum number of reflections, which is possible to be traced in the simulation, is critical to decide the computational complexity of the ray-tracing method. When the more number of reflections is considered, the simulation spends an exponentially more time although the prediction of the multipath channel is more precise. The maximum value is determined by preliminary tests that confirm the reasonable execution time and the simulation results that are almost same when the number of reflection is

counted up to five or more.

The UTD-based UBS model on a single path is applied according to the three random factors, namely the shadowing angle θ, the receiving antenna distance d, and the radius R, as mentioned earlier. All these three factors are uniformly distributed in the intervals of 0° to 360°, 0.1 m to 0.3 m, and 0.18 m and 0.25 m, respectively. The set of these random variables, $\{\theta, d, R\}$, is generated independently 15,000 times; in other words, 15,000 total UBS losses L_{tot}^{UBS} in equation (4.1) are obtained for a single link. Finally, the frequency of our interest is 2.4 GHz.

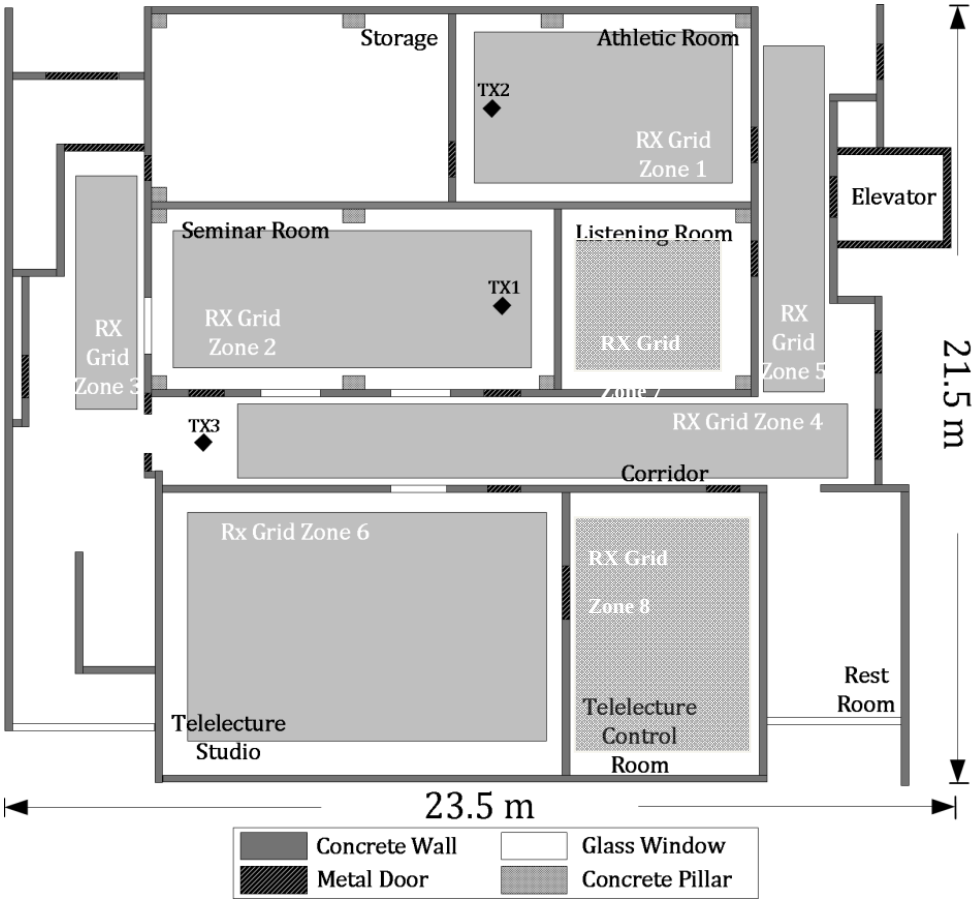

Figure 4.7 Floor plan of ray tracing in the laboratory building

4.4 Enhanced Statistical UBS Model

4.4.1 Bimodality in terms of K-factor

In this subsection, it is explored that how the bimodality characteristic of UBS changes according to K-factor. Furthermore, the criterion for grouping links is proposed based on the bimodality analysis. First, BC for each link is calculated from the data of the total UBS losses obtained by ray-tracing simulation. Figure 4.8 and 4.9 shows the distribution of BC versus K-factor for BM and TM, respectively. BC is evidently increased along with the increase in K-factor as explained in Section 4.2.1. The black solid line in Figure 4.8 and 4.9 is the criterion of bimodality suggestion based on BC.

However, from the point of view of the system, the criterion of bimodality needs to be the parameter of which value is known to the system such as K-factor. So, the proportion of bimodality suggestion that is BC over than 0.555 is calculated according to moving window of K-factor. The width of window is 2 dB and the step size of moving is 0.2 dB. As shown in Figure 4.10, the proportions of bimodality suggestion for both BM and TM largely monotonically increase along with K-factor. The criteria of K-factor in terms of proportion level are shown in Table 4.1.

First of all, the proportion level as criterion of link grouping have to be determined. The level of 50% can be the most rational choice, but links which have K-factor less than -5.2 dB in TM are too few to establish a representative model. On the other hand, the level of 70% is excessive because links of which UBS distributions are definitely bimodal are included in the unimodal

group. Consequently, the proportion level of 60% is adopted as criterion to distinguish the unimodal and bimodal groups appropriately.

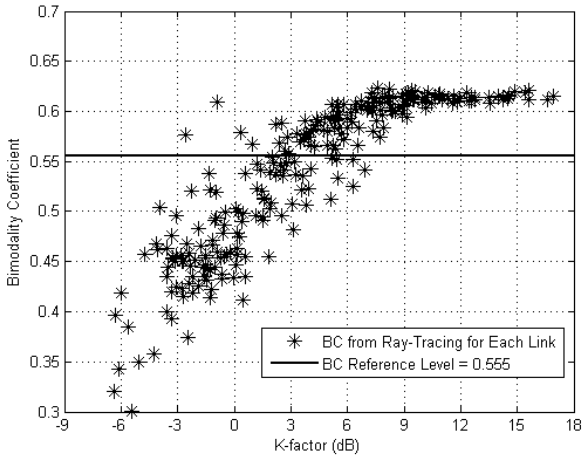

Figure 4.8 Relationship between BC and K-factor for BM

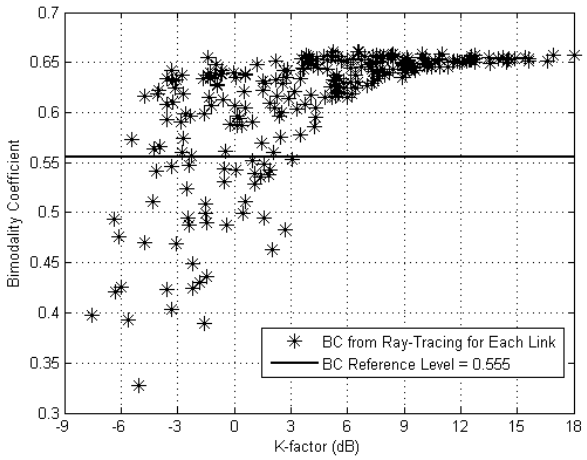

Figure 4.9 Relationship between BC and K-factor for TM

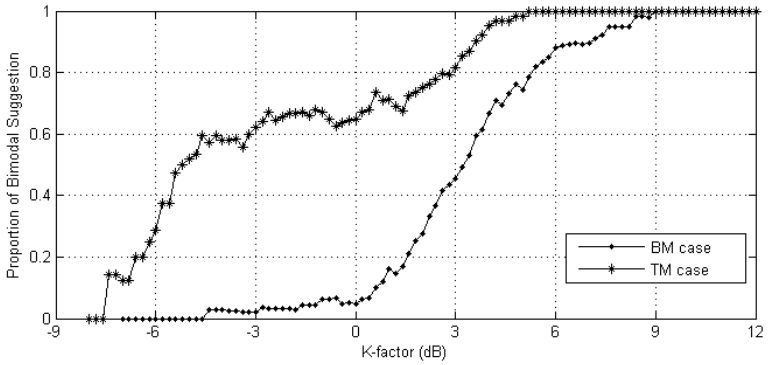

Figure 4.10 Proportion of bimodality suggestion based on BC

Table 4.1 K-factor criterion for bimodality depending on proportion level

Proportion Level	BM	TM
50%	3.3 dB	-5.2 dB
60%	**3.6 dB**	**-3.0 dB**
70%	4.5 dB	1.5 dB

4.4.2 The Unimodal UBS Model

Adopting the proportion level of 60%, the total UBS losses for links with K-factor lower than 3.6 dB for BM and -3.0 dB for TM are each grouped together to establish a representative unimodal model. The distribution of the total UBS losses and the fitting results by the maximum likelihood estimation with three different well-known probability distributions, that is Gaussian (normal), Rician, and Nakagami-*m* distributions, are presented in Figure 4.11 and 4.12. The difference of goodness-of-fit among the distributions is very marginal based on the log-likelihood values. In addition, it is remarkable that the UBS distributions for BM have the peak at nearby $L_{tot}^{UBS} = 1.0$, which indicates that there is no loss due to the UBS effect. In other words, the links with K-factor less than 3.6 dB are relatively unaffected by the UBS due to the multipath which have enough power to compensate for shadowing loss of blocked paths. On the other hand, the peak of UBS distributions for TM is at approximately $L_{tot}^{UBS} = 1.5$, which means that rather the received signal obtains the gain caused by the user with fairly high probability.

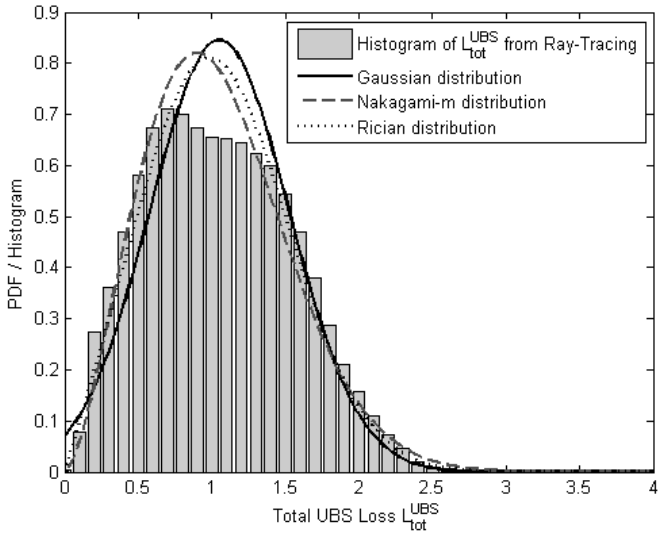

(a)

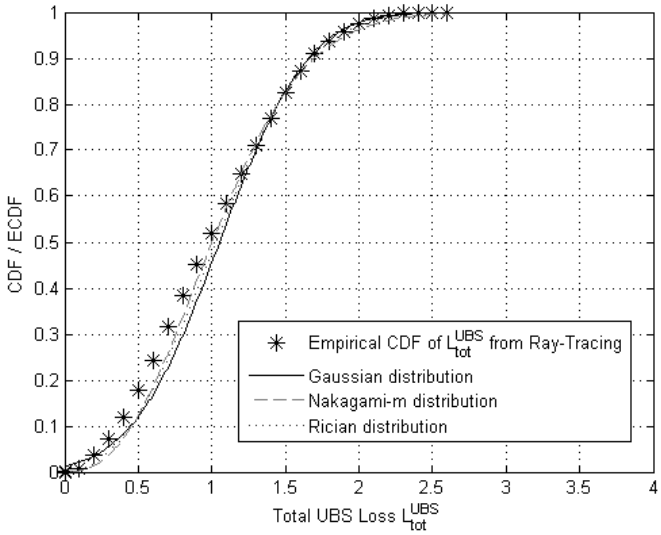

(b)

Figure 4.11 The distribution of the total UBS losses and the candidates for the unimodal UBS model in BM: (a) PDF and (b) CDF

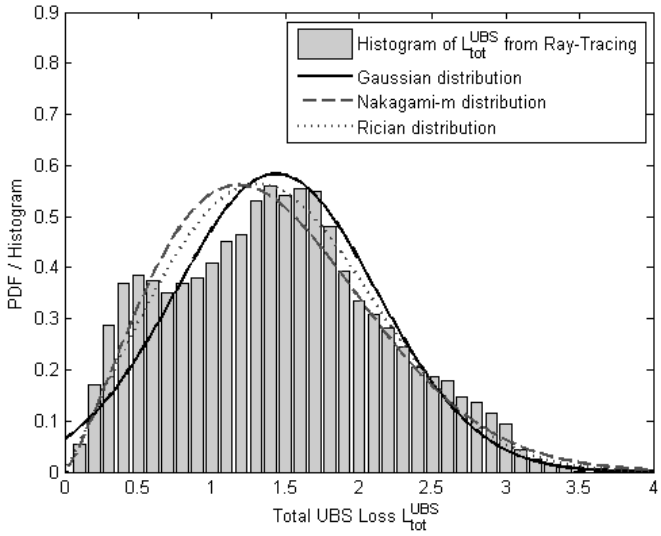

(a)

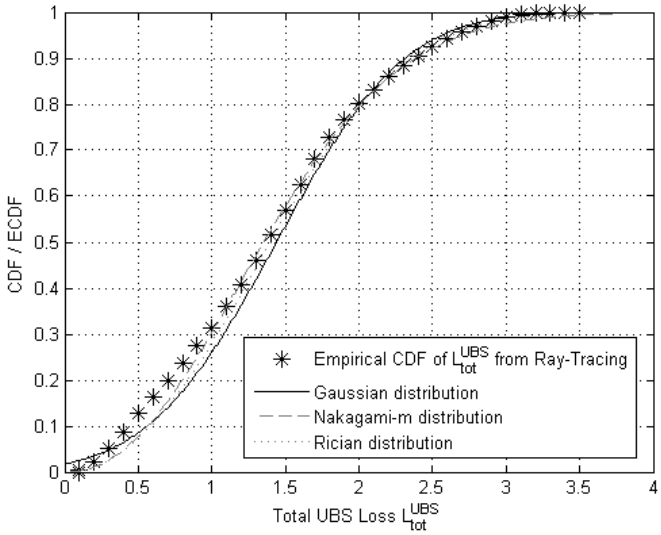

(b)

Figure 4.12 The distribution of the total UBS losses and the candidates for the unimodal UBS model in TM: (a) PDF and (b) CDF

4.4.3 The Bimodal UBS Model

In contrast to the unimodal models, the histograms of the total UBS losses for links with K-factor higher than the threshold (3.6 dB for BM and -3.0 dB for TM) are presented which obviously have bimodal shapes as shown in Figure 4.13 and 4.14. Finally, a GMM is used to establish the representative UBS model [43]. The GMM is a parametric PDF represented as a weighted sum of Gaussian component densities. The PDF of GMM is written as

$$f_{GMM}(x) = (1-\pi)g_1(x) + \pi g_2(x) \tag{4.3}$$

where π is a mixing proportion which has non-zero value for a bimodal model, whereas zero for a unimodal model; $g_j(x)$ is a PDF of Gaussian distribution with mean μ_j and variance σ_j^2. The set of parameters for the two-component GMM, $\{\pi, \mu_1, \sigma_1^2, \mu_2, \sigma_2^2\}$, is estimated using the iterative expectation maximization (EM) algorithm. The EM algorithm has a two-step iterative procedure using the log-likelihood function. The EM is a particular way to provide an implementable solution which converges to the maximum likelihood estimate [44]. Consequently, the GMM with the estimated parameters can describe much more precisely the UBS distributions than the Nakagami-*m* distribution model as shown in Figure 4.13 and 4.14. Finally, the estimated parameters of the unimodal and bimodal models are summarized in Table 4.2 and 4.3 for BM and TM, respectively.

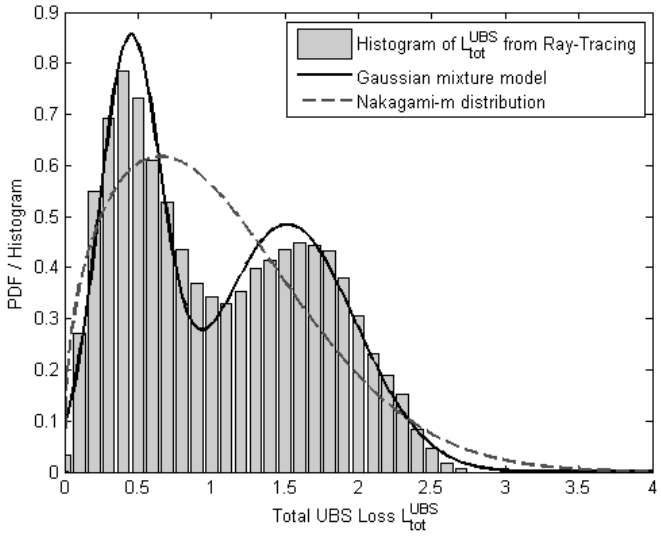

(a)

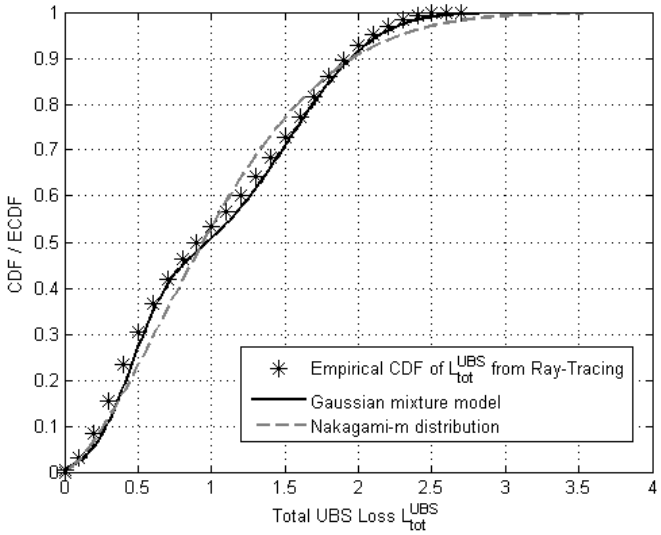

(b)

Figure 4.13 The distribution of the total UBS losses and the candidates for the bimodal UBS model in BM: (a) PDF and (b) CDF

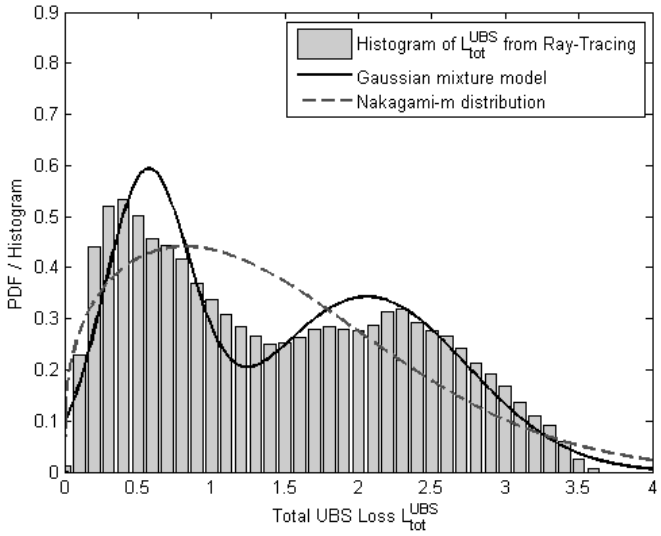

(a)

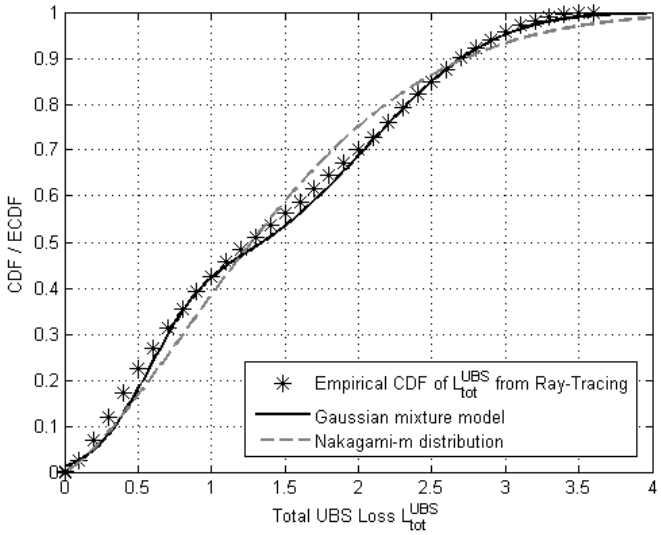

(b)

Figure 4.14 The distribution of the total UBS losses and the candidates for the bimodal UBS model in TM: (a) PDF and (b) CDF

Table 4.2 Estimated parameters of the unimodal and bimodal GMMs for BM

Unimodal	GMM	$\pi = 0$
	$G_1(x) \sim N(\mu_1, \sigma_1^2)$	$\mu_1 = 1.0513,\ \sigma_1 = 0.4970$
Bimodal	GMM	$\pi = 0.5674$
	$G_1(x) \sim N(\mu_1, \sigma_1^2)$	$\mu_1 = 0.4435,\ \sigma_1 = 0.0442$
	$G_2(x) \sim N(\mu_2, \sigma_2^2)$	$\mu_2 = 1.5143,\ \sigma_2 = 0.2184$

Table 4.3 Estimated parameters of the unimodal and bimodal GMMs for TM

Unimodal	GMM	$\pi = 0$
	$G_1(x) \sim N(\mu_1, \sigma_1^2)$	$\mu_1 = 1.4372,\ \sigma_1 = 0.7091$
Bimodal	GMM	$\pi = 0.5859$
	$G_1(x) \sim N(\mu_1, \sigma_1^2)$	$\mu_1 = 0.5584,\ \sigma_1 = 0.0863$
	$G_2(x) \sim N(\mu_2, \sigma_2^2)$	$\mu_2 = 2.0573,\ \sigma_2 = 0.4644$

4.5 Application of the Proposed Model for Other Environments

In this subsection, the UBS models proposed in Table 4.2 are compared with the UBS distributions obtained by ray-tracing simulation in three different environments in order to convince the reusability of the proposed model. The three sites are office, laboratory, and apartment building, respectively. For each site, approximately 300 links are investigated by ray-tracing simulation in the same way as in Section 4.3. In BM, as shown in Figure 4.15, the enhanced UBS models coincide with the results from other environments although the unimodal model of apartment which is the left figure in Figure 4.15(c) has some offsets in the vicinity of peak. The unimodal UBS distribution of the apartment environment is more concentrated on the peak because the apartment has the densest multipath channel due to the most complex structure among all the environments. It means that links with low K-factor in the apartment is least affected by UBS because of rich multipaths. On the other hand, all bimodal cases are considerably well fitted enough to assure of reusability. Also, in TM, the proposed UBS models are well matched with the UBS distributions in other environments as shown in Figure 4.16.

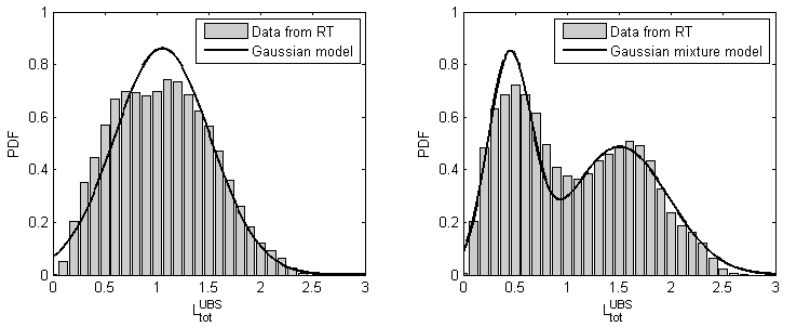

(a)

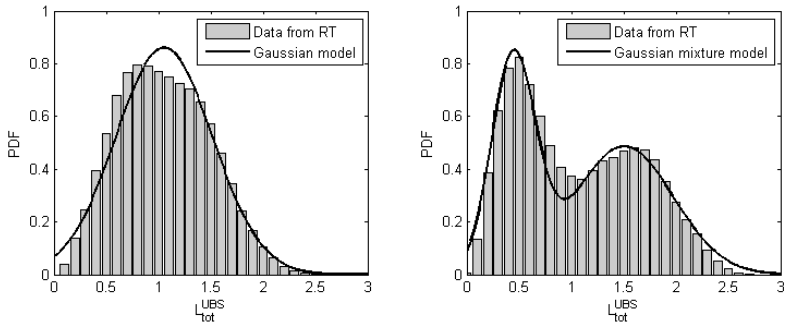

(b)

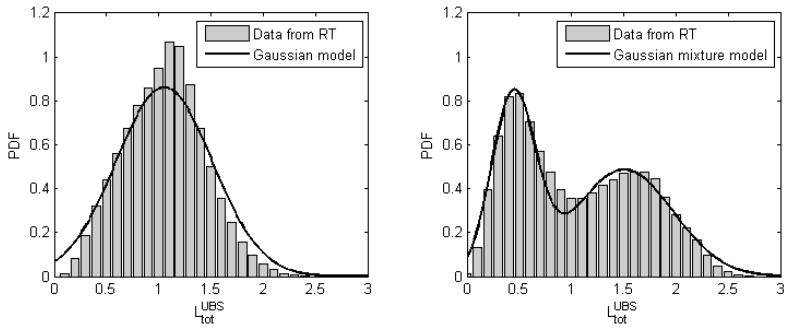

(c)

Figure 4.15 Applicability of the unimodal (left figures) and the bimodal (right figures) UBS models for BM to various types of indoor wireless channels: (a) office, (b) laboratory, and (c) apartment

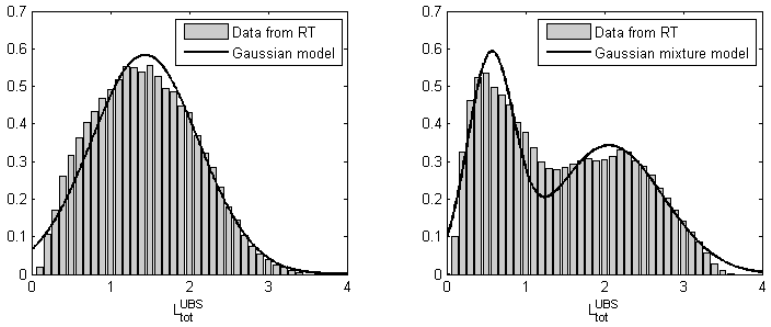

(a)

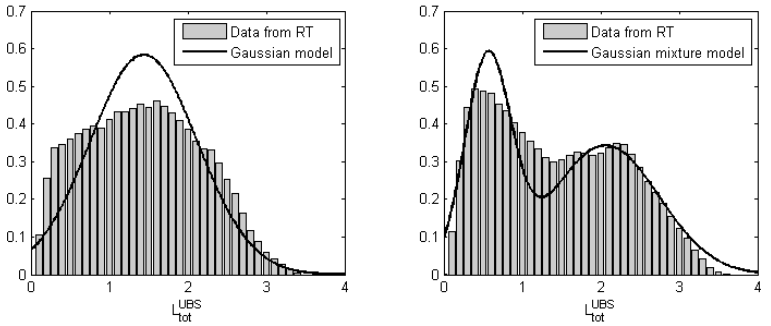

(b)

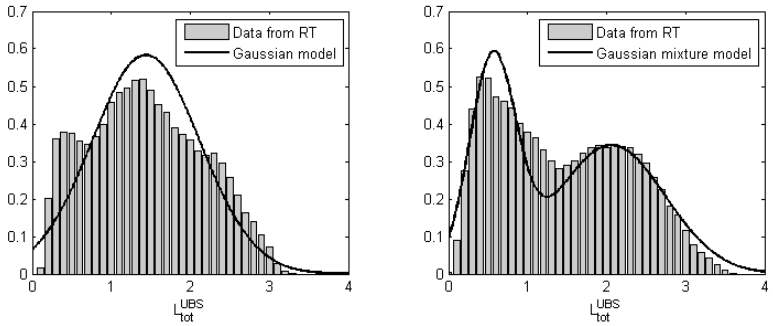

(c)

Figure 4.16 Applicability of the unimodal (left figures) and the bimodal (right figures) UBS models for TM to various types of indoor wireless channels: (a) office, (b) laboratory, and (c) apartment

4.5 Conclusion

In this chapter, the UBS models enhnaced from the previous Nakagami-*m* distribution models are proposed. The distribution of the total UBS losses has different stochastic properties depending on K-factor that is the main indicator to decide the UBS effect on propagation channel. Specifically, the UBS distribution was classified into a unimodal and bimodal type with the decision criterion of K-factor. The criterion of K-factor is determined based on the proportion level of bimodality suggestion adopted by 60 % in this research. For K-factor less than the threshold level, the UBS effect had relatively low impact on links, which was described as the unimodal model with Rician or Nakagami-*m* distribution. On the contrary, the bimodal UBS model established by GMM was applied to links with K-factor more than the threshold where UBS strongly influences the propagation channels. As a result, the total UBS losses in the bimodal models were most frequent at approximately 0.5 for both modes. Furthermore, the validity of these proposed models is verified using the raytracing simulation in various indoor environments.

Chapter 5. Conclusion

5.1 Summary

In this dissertation, the UBS effects on multipath propagation channels are investigated by using the ray-based techniques comprising the following steps. First, the shadowing effects depending on the states and relative positions of the user are examined to determine the power loss on a single propagation path based on the UTD. Next, the UTD-based model is combined with the multipath channel profiles obtained from the ray-tracing. Finally, the total UBS loss which means the additional path loss factor cause by the UBS is defined, and the distributions of total UBS loss are statistically characterized taking into consideration the randomness of the user's positions. At first, the UBS distributions at each link are described by Nakagami-*m* distribution, and its parameters are proposed as a function of K-factor. However, since the Nakagami-*m* model has a drawback of inaccuracies for the links with high K-factor, the enhanced UBS models are newly proposed based on the bimodal characteristics of UBS distributions. Specifically, the UBS distributions were classified into unimodal and bimodal groups with the decision criterion of K-factor. Rician and Nakagami-*m* models well describe the UBS distributions for the unimodal group and GMM is proposed for the bimodal one.

5.2 Expansion and Application of User Body Effects

5.2.1 Other Frequency Bands

The UTD and ray-tracing technique are valid under the high-frequency assumption that includes most of frequency bands occupied by the current commercial wireless communication systems. From hundreds of MHz to approximately 10 GHz, the methodology of this dissertation is simply possible to be utilized. However, over 10 GHz bands such as millimeter waves and terahertz, the ray-based methodology is not appropriate. In these frequency bands, the human bodies are not regarded as smooth surface anymore because the order of wavelength is too short to ignore the tiny variation of surface such as roughness of cloth and small accessories. The waves in these bands are diffused irregularly by the surface. Consequently, other approach is requested to analyze the human body effects on frequency bands over tens of GHz. Figure 5.1 shows the UTD scattering results at typical frequencies within few GHz.

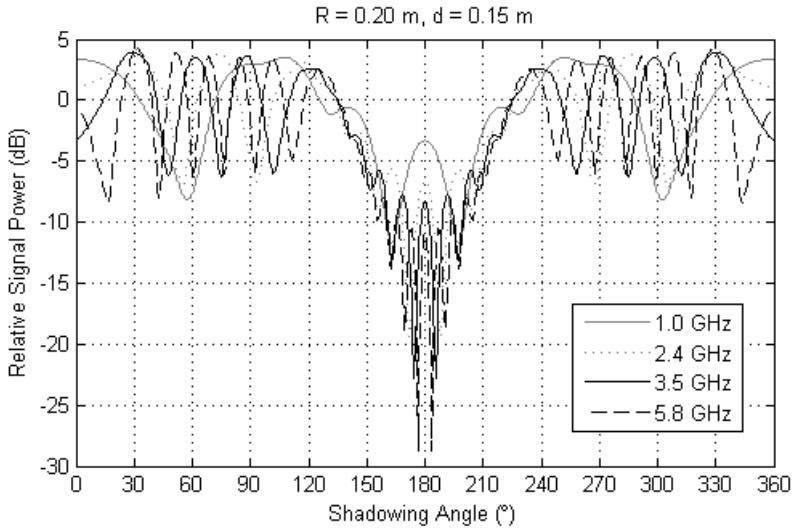

Figure 5.1 UTD scattering solution at various frequencies

5.2.2 Device-to-device (D2D) Communications

With a drastic growth of smart handset devices, user demands for high data rate are also increasing unprecedentedly. The applications with high data contents are already pushing current cellular systems to the limits on the maximum rates at which can be obtained in the systems. D2D communication has recently regarded as one promising method to supplement cellular networks. Although D2D communication basically means that mobile devices directly communicate without cellular network infrastructure, the D2D systems controlled by the existing network infrastructure are also being designed by communication operators.

D2D communications generally assume the situation that the mobile devices are very close. With high probabilities, D2D links are LOS and have

high K-factor, which means that the links are very sensitive to the effects of user bodies according to the results of this dissertation [45].

The analysis of this dissertation can be utilized for the D2D control link between the mobile device and the base station or access point. However, for application to the typical D2D communications between two mobile devices, the expansion to effects of two user bodies is needed, which can be achieved by using the UTD solutions for multiple convex surfaces [28], [46]. Distributions of the total UBS loss in the case of two bodies which are the users at both ends of a link are shown in Figure 5.2 and 5.3. The fitting models using GMM show still good accuracy, but the distributions are closer to log-normal shape, not bimodal shape. The log-normal distribution generally describes signal variations in shadow-rich environments. By the additional body, the probability that the direct path of a link is blocked by the user bodies is increased and the bimodal characteristics in one body cases are weaken.

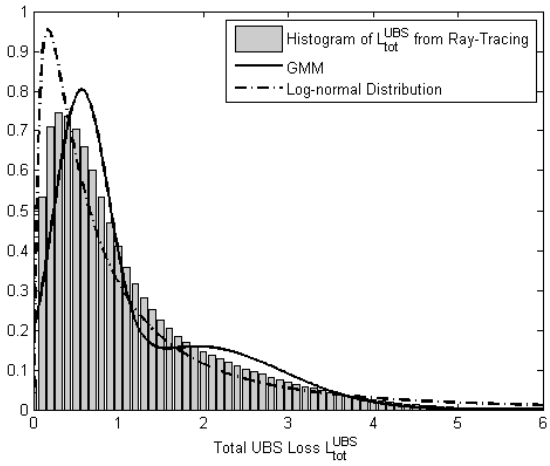

(a)

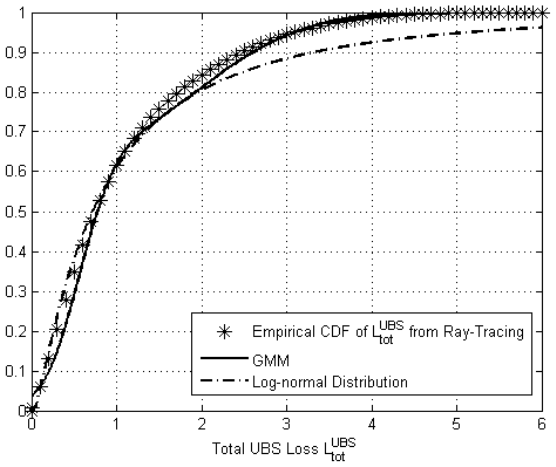

(b)

Figure 5.2 The distribution of the total UBS losses for two user bodies in BM:

(a) PDF and (b) CDF

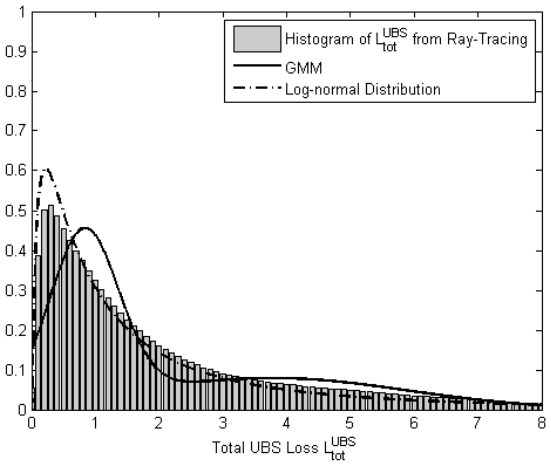

(a)

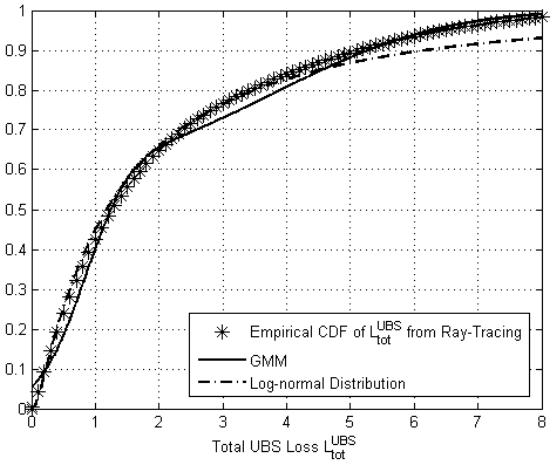

(b)

Figure 5.3 The distribution of the total UBS losses for two user bodies in TM: (a) PDF and (b) CDF

5.2.3 Temporal Variation of UBS

It is essential to evaluate the temporal variation of UBS owing to change in position or posture of user considering realistic communications. In practical situation, the position or posture of user changes in real time, but it might be characterized depending on circumstance. For example, the D2D communications mentioned above are possible to restrict the user's position or movement because they are mainly connected in close proximity of devices. However, the ray-based deterministic approaches have limits to analysis time-varying effects. The field measurements in accordance with scenarios have to be combined with those deterministic methods.

Bibliography

[1] H. L. Bertoni, Radio Propagation for Modern Wireless Systems. Prentice-Hall, Upper Saddle River, NJ, 2000.

[2] H. Hashemi, “The Indoor Radio Propagation,” in Proc. IEEE, vol. 81, no. 7, pp. 943-968, July 1993.

[3] A. A. M. Saleh and R. A. Valenzuela, “A Statistical Model for Indoor Multipath Propagation,” IEEE J. Sel. Areas Commun., vol. 5, no. 2, pp. 128-137, Feb. 1987.

[4] R. J. C. Bultitude, “Measurement, Characterization and Modeling of Indoor 800/900 MHz Radio Channels for Digital Communications,” IEEE Commun. Mag., vol. 25, no. 6, pp. 5-12, June 1987.

[5] S. C. Kim, H. L. Bertoni, and M. Stern, “Pulse Propagation Characteristics at 2.4 GHz Inside Buildings,” IEEE Trans. Veh. Technol., vol. 45, no. 3, pp. 579-592, Aug. 1996.

[6] H. Xu, V. Kukshya, and T. S. Rappaport, “Spatial and Temporal Characteristics of 60-Ghz Indoor Channels,” IEEE J. Sel. Areas Commun., vol. 20, no. 3, pp. 620-630, Apr. 2002.

[7] A. F. Molisch, “Ultrawideband Propagation Channels - Theory, Measurement, and Modeling,” IEEE Trans. Veh. Technol., vol. 54, no. 5, pp.

1528-1545, Sep. 2005.

[8] Y. Wang, S. S. Naeini, and S. K. Chaudhuri, “A Hybrid Technique Based on Combining Ray Tracing and FDTD Methods for Site-Specific Modeling of Indoor Radio Wave Propagation,” IEEE Trans. Antennas Propag., vol. 48, no. 5, pp. 743-754, May 2000.

[9] Y. Zhao, Y. Hao, and C. Parini, “FDTD Characterization of UWB Indoor Radio Channel Including Frequency Dependent Antenna Directivities,” IEEE Antennas Wirel. Propag. Lett., vol. 6, pp. 191-19, 2007.

[10] A. O. Kaya, L. J. Greenstein, and W. Trappe, “Characterizing Indoor Wireless Channels via Ray Tracing Combined with Stochastic Modeling,” IEEE Trans. Wireless Commun., vol. 8, no. 8, pp. 4165-4175, Aug. 2009.

[11] W. Honcharenko, H. L. Bertoni, J. L. Dailing, J. Qian, and H. D. Yee, "Mechanisms Governing UHF Propagation on Single Floors in Modern Office Buildings," IEEE Trans. Veh. Technol., vol. 41, no. 4, pp. 496-504, Nov. 1992.

[12] S. C. Kim et al., "Radio Propagation Measurements and Prediction Using Three-Dimensional Ray Tracing in Urban Environments at 908 MHz and 1.9 GHz," IEEE Trans. Veh. Technol., vol. 48, no. 3, pp. 931-946, May 1999.

[13] J. W. McKwon and Jr. R. L. Hamilton, “Ray Tracing as a Design Tool for Radio Networks,” IEEE Netw., vol. 5, no. 6, pp. 27-30, Nov. 1991.

[14] R. A. Valuenzuela, “A Ray Tracing Approach to Predicting Indoor

Wireless Transmission," in Proc. IEEE the 43rd Veh. Technol. Conf., pp. 214-218, 1993.

[15] S. J. Fortune, D. M. Gay, B. W. Kernighan, O. Landron, R. A. Valenzuela, and M. H. Wright, "WISE Design of Indoor Wireless System: Practical Computation and Optimization," IEEE Comput. Sci. Eng., vol. 2, pp. 58-68, 1995.

[16] G. E. Athanasiadou, and A. R. Nix, "A Novel 3-D Indoor Ray-Tracing Propagation Model: The Path Generator and Evaluation of Narrow-Band and Wide-Band Predictions," IEEE Trans. Veh. Technol., vol. 49, no. 4, pp. 1152-1168, July. 2000.

[17] K. A. Remley, H. R. Anderson, and A. Weisshar, "Improving the Accuracy of Ray-tracing Techniques for Indoor Propagation Modeling," IEEE Trans. Veh. Technol., vol. 49, no. 6, pp. 2350-2358, Nov. 2000.

[18] S. Obayashi, and J. Zander, "A Body-Shadowing Model for Indoor Radio Communication Environments," IEEE Trans. Antennas Propag., vol. 46, no. 6, pp. 920-927, Jun. 1998.

[19] J. Toftgard, S. N. Hornsleth, and J. B. Andersen, "Effects on Portable Antennas of the Presence of a Person," IEEE Trans. Antennas Propag., vol. 41, no. 6, pp. 739-746, Jun. 1993.

[20] M. Okoniewski and M. A. Stuchly, "A Study of the Handset Antenna and

Human Body Interaction," IEEE Trans. Microw. Theory Tech., vol. 44, no. 10, pp. 1855-1864, Oct. 1996.

[21] I. Kashiwagi, T. Taga, and T. Imai, "Time-Varying Path-Shadowing Model for Indoor Populated Environments," IEEE Trans. Veh. Technol., vol. 59, no. 1, pp. 16-28, Jan. 2010.

[22] F.-L. Lin and H.-R. Chuang, "Performance Evaluation of a Portable Radio Close to the Operator's Body in Urban Mobile Envrionements," IEEE Trans. Veh. Technol., vol. 49, no. 2, pp. 614-621, Mar. 2000.

[23] F. Harrysson, J. Medbo, A. F. Molisch, A. J. Johansson, and F. Tufvesson, " Efficient Experimental Evaluation of a MIMO Handset with User Influence," IEEE Trans. Wireless Commun., vol. 9, no. 2, pp. 853-863, Mar. 2000.

[24] J. Ø. Nielsen, B. Yanakiev, I. B. Bonev, M. Christensen, and G. F. Pedersen, "User Influence on MIMO Channel Capacity for Handsets in Data Mode Operation," IEEE Trans. Antennas Propag., vol. 60, no. 2, pp. 633-643, Feb. 2012.

[25] P. V. Torre, L. Vallozzi, L. Jacobs, H. Rogier, M. Moeneclaey, and J. Verhaevert, "Characterization of Measured Indoor Off-Body MIMO Channels with Correlated Fading, Correlated Shadowing and Constant Path Loss," IEEE Trans. Wireless Commun., vol. 11, no. 2, pp. 712-721, Feb. 2012.

[26] A. Fort, F. Keshmiri, G. R. Crusats, C. Craeye, and C. Oestges, “A Body Area Propagation Model Derived from Fundamental Principles: Analytical Analysis and Comparison with Measurements,” IEEE Trans. Antennas Propag., vol. 58, no. 2, pp. 503-514, Feb. 2010.

[27] S. L. Cotton and W. G. Scanlon, “An Experimental Investigation into the Influence of User State and Environment on Fading Characteristics in Wireless Body Area Networks at 2.45GHz,” IEEE Trans. Wireless Commun., vol. 8, no. 1, pp. 6-12, Jan. 2009.

[28] G. Koutitas, “Multiple Human Effects in Body Area Networks,” IEEE Antennas Wireless Propag. Lett., vol. 9, pp. 938-941, Oct. 2010.

[29] P. S. Hall and Y. Hao, Antennas and Propagation for Body-Centric Wireless Communications. Artech House, Norwood, MA, 2006.

[30] M. Ghaddar, L. Talbi, T. A. Denidni, and A. Sebak, “A Conducting Cylinder for Modeling Human Body presence in Indoor Propagation Channel,” IEEE Trans. Antennas Propag., vol. 55, no. 11, pp. 3099-3103, Nov. 2007.

[31] J. B. Keller, “Geometrical Theory of Diffraction,” J. Opt. Soc. Am., vol. 52, pp. 116-130, 1962.

[32] J. B. Keller, “Diffraction by a Convex Cylinder,” IRE Trans. Antennas and Propagation, vol. AP-24, pp. 312-321, 1956.

[33] R. G. Kouyoumjian and P. H. Pathak, “A Uniform Geometrical Theory of Diffraction for an Edge in a Perfectly Conducting Surface,” in Proc. IEEE, vol. 62, pp. 1448-1461, Nov. 1974.

[34] P. H. Pathak, W. D. Burnside, and R. J. Marhefka, “A Uniform GTD Analysis of the Diffraction of Electromagnetic Waves by a Smooth Convex Surface,” IEEE Trans. Antennas Propag., vol. 28, no. 5, pp. 631-642, Sep. 1980.

[35] D. A. McNamara, C. W. Pisturius, and J. A. Malherbe, Introduction to the Uniform Geometrical Theory of Diffraction. Norwood, MA: Artech House, 1990.

[36] R. Paknys, “On the Accuracy of the UTD for the Scattering by a Cylinder,” IEEE Trans. Antennas Propag., vol. 42, no. 5, pp. 757-760, May 1994.

[37] T. Funkhouser, N. Tsingos, I. Carlbom, G. Elko, M. Sondhi, J. E. West, G. Pingali, P. Min, and A. Ngan, “A Beam Tracing Method for Interactive Architectural Acoustics”, J. Acoust. Soc. Am., vol. 115, no. 2, pp. 739-756, 2004.

[38] J. D. Parsons, The Mobile Radio Propagation Channel. Wiley, New York, NY, 1992.

[39] M. Nakagami, “The *m*-distribution: A General Formula of Intensity

Distribution of Rapid Fading," in Statistical Methods in Radio Wave Propagation, W. C. Hoffman, Ed. New York: Pergamon, 1960, pp. 3-36.

[40] J.-H. Jung, J. Lee, J.-H. Lee, Y.-H. Kim, and S.-C. Kim, "Ray-tracing-aided modeling of user-shadowing effects in indoor wireless channels," IEEE Trans. Antennas Propag., vol. 62, no. 6, pp. 3412-3416, Jun. 2014.

[41] A. Fort, C. Desset, P. D. Doncker, P. Wambacq, and L. V. Biesen, "An Ultra-Wideband Body Area Propagation Channel Model - From Statistics to Implementation," IEEE Trans. Microw. Theory Tech., vol. 54, no. 4, pp. 1820-1826, Apr. 2006.

[42] J. B. Freeman and R. Dale, "Assessing Bimodality to Detect the Presence of a Dual Cognitive Process," Behavior Research Methods, vol. 45, no. 1, pp. 83-97, 2013.

[43] D. A. Reynolds and R. C. Rose, "Robust Text-Independent Speaker Identification Using Gaussian Mixture Speaker Models," IEEE Trans. Speech Audio Process., vol. 3, no. 1, pp. 72-83, Jan. 1995.

[44] C. N. Georghiades and J. C. Han, "Sequence Estimation in the Presence of Random Parameters via the EM Algorithm," IEEE Trans. Commun., vol. 45, no. 3, pp. 300-308, Mar. 1997.

[45] S. L. Cotton, "Human Body Shadowing in Cellular Device-to-Device Communications: Channel Modeling Using the Shadowed κ-μ Fading

Model," IEEE J. Sel. Areas Commun., vol. 33, no. 1, pp. 111-119, Jan. 2015.

[46] G. Koutitas and C. Tzaras, "A UTD Solution for Multiple Rounded Surfaces," IEEE Trans. Antennas Propag., vol. 54, no. 4, pp. 1277-1283, Apr. 2006.

초 록

본 논문에서는 단말기 사용자가 실내 무선 채널에서 신호 전파에 미치는 영향을 분석한다. 사용자는 거의 모든 시간에 걸쳐 단말기에 매우 가까이 위치하여 신호 전파에 지속이고 강력한 영향을 미친다. 따라서 채널 내에 존재하는 다른 인체의 영향과는 구분하여, 단말기 사용자가 전파 채널에 미치는 영향을 분석할 필요가 있다. 본 논문에서는 균일 회절 이론 (UTD)과 광선 추적 기법을 활용하여 주파수 2.4 GHz 대역에서의 단말기 사용자 쉐도잉 영향에 대해 조사한다.

우선적으로, 단일 전파 경로에서 대한 사용자 쉐도잉을 UTD를 이용하여 결정론적으로 모델링한다. UTD 산란 모델은 매끈한 곡면에서 발생하는 신호 회절에 대한 해를 제공하는데, 본 논문에서는 원통형으로 가정된 사용자의 영향 분석을 위해 UTD 산란 모델을 채택하였다. UTD 기반의 단일 전파 경로에 대한 사용자 쉐도잉 모델은 사용자의 상대적인 위치에 따른 수신 신호 손실로 정의된다. 이 UTD 기반의 사용자 쉐도잉 모델은 전파 무향실 실험 결과와의 비교를 통하여 검증하였다.

위와 같이 검증된 UTD 기반 모델을 실내 광선 추적 기법과 연동하여 다중 경로 채널에서의 사용자 쉐도잉 영향을 조사한다. 광선 추적 기법은 다중경로들의 수신 전력뿐만 아니라 각도 정보까지 제공하기 때문에, 사용자의 위치와 다중 경로 광선들의 방향이 이루는 상대적인 값에 따라 UTD 기반의 단일 전파 경로

모델을 적절히 적용할 수 있다. UTD 기반 모델과 광선 추적 기법의 연동 결과 또한 실내 측정 실험 결과와의 비교를 통하여 검증하였다.

하지만, 현실적인 통신 환경에서는 사용자의 위치가 어느 특정한 곳에 고정되어 있기 어려울 뿐만 아니라, 사용자 위치에 대한 정보를 시스템이 실시간으로 알 수 없기 때문에 결정론적인 사용자 쉐도잉 모델을 활용하기에는 부적합하다. 따라서 사용자의 위치 변화에 대한 임의성을 고려하여 통계적인 사용자 쉐도잉 모델을 도출하였다. 우선적으로 K팩터를 사용자 쉐도잉의 정도를 결정하는 가장 중요한 파라미터로 제시하였다. K팩터는 다중 경로 환경에서 가장 점유율이 큰 경로의 신호 세기와 나머지 경로들의 신호 세기의 합에 대한 비율로서 정의된다. 다중 경로 환경에서 사용자 쉐도잉의 양은 다중 경로 중에서 가장 점유율이 큰 경로가 사용자에 의해서 가려졌는지 여부와 그 경로의 점유율 정도에 따라 크게 달라지므로 K팩터가 사용자 쉐도잉 영향을 결정하는 적절한 파라미터라고 할 수 있다. 결과적으로, 광선 추적 기법 모의실험을 통하여 얻은 각 링크에서의 사용자 쉐도잉에 의한 총 수신 신호 손실의 분포를 Nakagami-*m* 분포를 이용하여 모델링하였다. Nakagami-*m* 분포의 파라미터는 *m*은 K팩터에 대한 함수 형태로 제시하였다.

마지막으로, 보다 개선된 형태의 통계적 사용자 쉐도잉 모델을 제시하였다. Nakagami-*m* 분포를 기반으로 한 사용자 쉐도잉 모델을 높은 K팩터 값을 갖는 링크에서 정확도가 떨어진다는 단점을 보이는데, 높은 K팩터 값을 갖는 링크에서는 사용자 쉐도잉에 의한 신호 손실의 분포가 양봉 분포의 특성을 띄기 때문이다. 따라서 사용자 쉐도잉에 의한 신호 손실의 분포 형태에 따라 단봉 그룹과

양봉 그룹으로 구분하고, 각 그룹을 대표하는 통계적 사용자 쉐도잉 모델을 제시하였다. 단봉 모델에서는 Rician 분포가 가장 정확한 것으로 나타났고, 양봉 모델을 위해서는 가우시안 혼합 모델을 사용하였다. 개선된 통계적 사용자 쉐도잉 모델은 다른 실내 환경들에서의 광선 추적 기법 결과와 비교를 통해 검증하였다.

주요어 : 광선 추적 기법, 균일 회절 이론, 사용자 쉐도잉 영향, 실내 무선 채널, 양봉 분포

학번 : 2008-20973